

Evolution of Vacuum Fluctuations of an Ultra-Light Massive Scalar Field generated during and before Inflation

Hajime Aoki^a and Satoshi Iso^{b,c}

^a*Department of Physics, Saga University, Saga 840-8502, Japan*

^b*KEK Theory Center, High Energy Accelerator Research Organization (KEK),
Ibaraki 305-0801, Japan*

^c*Graduate University for Advanced Studies (SOKENDAI),
Ibaraki 305-0801, Japan*

Abstract

We consider an ultra-light scalar field with a mass comparable to (or lighter than) the Hubble parameter of the present universe, and calculate the time evolution of the energy-momentum tensor of the vacuum fluctuations generated during and before inflation until the late-time radiation-dominated and matter-dominated universe. The equation of state changes from $w = 1/3$ in the early universe to $w = -1$ at present, and it can give a candidate for the dark energy that we observe today. It then oscillates between $w = -1$ and 1 with the amplitude of the energy density decaying as a^{-3} . If the fluctuations are generated during ordinary inflation with the Hubble parameter $H_I \lesssim 10^{-5} M_{\text{Pl}}$, where M_{Pl} is the reduced Planck scale, we need a very large e-folding number $N \gtrsim 10^{12}$ to explain the present dark energy of the order of 10^{-3}eV . If a Planckian universe with a large Hubble parameter $H_P \sim M_{\text{Pl}}$ existed before the ordinary inflation, an e-folding number $N \sim 240$ of the Planckian inflation is sufficient.

1 Introduction

Our universe is well described by the spatially flat Λ cold dark matter (Λ CDM) model. According to the PLANCK 2013 results [1], only 5.1% of the energy density is attributed to a known form of baryonic matter, while 26.8% is attributed to cold dark matter, and 68.3% to dark energy (DE). Although its equation of state $w(= p/\rho) = -1$ seems like that of vacuum energy of quantum fields, there is no reasonable explanation for its magnitude, $\rho_{\text{DE}} = 3(M_{\text{Pl}}H_0)^2\Omega_\Lambda \sim (2.2\text{meV})^4$, where $\text{meV} = 10^{-3}\text{eV}$. Here, $M_{\text{Pl}} = (8\pi G_N)^{-1/2} \sim 2.4 \times 10^{30}\text{meV}$ is the (reduced) Planck scale and $H_0 \sim 1.4 \times 10^{-30}\text{meV}$ is the current Hubble parameter. ρ_{DE} is far smaller than the expected magnitude of vacuum energy Λ^4 in a theory with an ultraviolet (UV) cutoff Λ . If we take Λ to be M_{Pl} , ρ_{DE} is smaller than Λ^4 by more than 120 orders of magnitude. This is the cosmological constant problem [2].

On the other hand, we may try to explain the dark energy as the Casimir energy in the current universe. In particular, the vacuum energy for fluctuations of massless fields in de Sitter background with Hubble parameter H is of order H^4 , and has $w = -1$ [3, 4]. Since our present universe is close to de Sitter space, one may wonder if dark energy can be explained as vacuum energy in de Sitter with the current Hubble parameter H_0 , but this does not seem to be plausible. Dark energy that we observe as $M_{\text{Pl}}^2 H_0^2$ is much larger than the expected contribution from a single field H_0^4 .

However, H_0 is not the only dimensionful quantity that affects the renormalized energy-momentum tensor (EMT). To compute the expectation values of fluctuations, we need to specify the vacuum state. This may depend on the global properties of the geometry and the whole history of the universe, and thus different scales might be introduced into the problem. There is by now strong evidence [5] that there has been a period of inflation with the Hubble parameter H_I much larger than H_0 . It would be reasonable to take the vacuum to be the Bunch-Davies (BD) vacuum [3] for de Sitter space with H_I . Fluctuations of a massless scalar in de Sitter background are of order H_I . Fluctuations are frozen (remain constant) outside the Hubble radius (see, e.g., Ref. [6]); thus, infrared (IR) modes could have a large value in the universe after inflation. In fact, these fluctuations are considered to be the origin of the fluctuations in the cosmic microwave background (CMB) that are observed today [1, 5].

In Refs. [7] and [8], the time evolution of the EMT is calculated for a minimally coupled massless scalar field. The fluctuations are generated during the inflationary universe and evolve until the late-time universe of the radiation-dominated (RD) and matter-dominated (MD) eras. The equation of state w

approaches $w = 1/3$ and $w = 0$ in the RD and MD periods, respectively. The magnitude of the present energy density is of order $H_I^2 H_0^2$, and is still much smaller than that of the dark energy in our universe. The analysis is extended to a non-minimally coupled scalar field in Ref. [9].

In order to circumvent the smallness of energy density, we considered a double inflation model in Ref. [8]. We assumed that there was an inflation with a Hubble parameter H_P of the order of the Planck scale M_{Pl} (which should be natural in, e.g., Starobinsky inflation [10]) before the usual inflation with H_I started. We fix the initial condition of the fields in the Planckian inflation period by taking a Bunch-Davies vacuum with the Hubble parameter H_P , and study the time evolution afterwards. In this case, the IR mode is enhanced to H_P , and the present value of vacuum energy becomes of order $H_P^2 H_0^2$. In order to make these large fluctuations consistent with the observed value of CMB fluctuations, the enhancement needs to be restricted in the far-IR modes whose wavelengths are larger than the current Hubble radius H_0^{-1} . Since the enhanced modes are still out of the horizon now and the dominant contribution to the EMT is given by the spacial-derivative parts $|\nabla\phi|^2$, the equation of state is given by $w = -1/3$ instead of $w = 1/3$ or $w = 0$ as in ordinary inflation.

In the present paper, we extend our previous analysis in Ref. [8] to an (ultra-light) massive scalar field. If the mass is smaller than the Hubble parameter $m \ll H_I$, the wave function is greatly enhanced during the inflation, as in the massless case. The low-momentum modes remain frozen until the mass becomes larger than the Hubble parameter in the late universe when the field starts to oscillate. Such ultra-light scalars have been studied extensively as candidates for dark matter (see Ref. [11] and papers citing Ref. [11]). The scenario has attracted renewed interest since Ref. [12]. For $m \gtrsim 10^{-24}\text{eV}$, it is indistinguishable from the standard cold dark matter [13]. For lighter mass $10^{-32}\text{eV} \lesssim m \lesssim 10^{-25.5}\text{eV}$, its abundance is strongly constrained by the CMB and galaxy-clustering data. If its mass is smaller than the current Hubble parameter $H_0 \sim 10^{-33}\text{eV}$, it could be a candidate for the dark energy at present [14, 15]. If the light particle is an axion-like particle, the initial value of the field is set by the misalignment mechanism, so the amplitude of the energy density can be chosen by hand. A similar idea is given by the quintessence scenario (for a review, see, e.g., Ref. [16]), where the initial value of the field is also set by hand. In this paper, we investigate the possibility that the initial field value is dynamically determined by the fluctuations generated during the primordial inflation.

A similar proposal was given in Ref. [17]. Using the saturated value $3H_I^4/16\pi^2$ of the energy density generated by an inflation with an infinite duration, or an

infinite e-folding, a tiny Hubble parameter $H_I \sim \text{meV}$ is required to explain the observed value of the dark energy. For an inflation with a finite e-folding number N , the energy density becomes $(m^2/2)(H_I/2\pi)^2 N$. For $m \lesssim H_0$ and $H_I \lesssim 10^{-5} M_{\text{Pl}}$, which is required by the CMB observation, we need a large e-folding number N to make this energy density comparable to the current dark energy. While the lower bound for N was given in Ref. [17] as $N \gtrsim 10^9$, we obtain a slightly different value $N \gtrsim 10^{12}$ by taking numerical factors into account. We also consider a different physical setting where we suppose a period of pre-inflation with a large Hubble parameter $H_P \sim M_{\text{Pl}}$ before the ordinary inflation starts. In this case, an e-folding number $N \sim 240$ for the Planckian inflation is sufficient.

The purpose of the present paper is twofold. One is, as we mentioned above, to give conditions to explain the present dark energy by the vacuum fluctuations generated during the inflation or pre-inflation, and to investigate the time evolution of the EMT through the RD and MD eras. We extend our analyses to see the behavior in the future when $m > H$ and the EMT behaves as a dust with an oscillating w , though the back reaction of the induced EMT to the geometry needs to be included. The second purpose is to obtain the *exact* wave function of a massive scalar field with the Bunch-Davies initial condition, for all the time and for all the momenta, and to calculate the EMT by using it. While analyses using only zero-momentum modes are often performed in the literature, our analyses contain nonzero-momentum modes as well. We also obtain some approximated forms of the wave function by applying the WKB approximation, and by using the power-expansion and asymptotic forms of the special functions describing the exact wave function. These results will serve as bases for future calculations, e.g., when interactions among different modes become important. Studies for the former purpose are mainly given in section 4, and those for the latter in sections 2 and 3.

Our results will shed light on the effect of almost massless and non-interacting scalar fields, such as axions. Although our work is related to the studies of fluctuations of gravitons or inflatons [18, 19, 20, 21, 22], further modifications are necessary since the EMT for gravitons has different tensor structures from the scalar fields. One should also study quantum fluctuations around the classical value of the inflaton field developed in the potential. We believe that our work serves as a starting point for a study of the effects of those fields.

The paper is organized as follows. In section 2, we solve the equation of motion of a massive scalar field in the history of the universe with the inflation period followed by the RD universe. In section 3, we calculate the EMT and study its time evolution. In section 4, we obtain the conditions in which

the vacuum fluctuation of the ultra-light scalar explains the dark energy at present. The last section, section 5, is devoted to conclusions and discussions. In Appendix A, we calculate the time evolution of the EMT by using the zero-momentum approximation. The time evolution in the MD period is given by using this approximation.

2 Massive scalars in an expanding universe

Our universe is approximated by the Robertson-Walker spacetime with the inflation, RD (radiation-dominated), and MD (matter-dominated) periods. In this section, we focus on the first two stages of the universe and study the detailed behaviors of the wave function of a massive scalar field.¹ The metric is given by $ds^2 = a(\eta)^2 [d\eta^2 - (dx^i)^2]$ in terms of the conformal coordinates (η, x^i) , and the scale factor $a(\eta)$ is given by

$$a(\eta) = \begin{cases} a_{\text{Inf}}(\eta) = -\frac{1}{H_I \eta} & (\eta_{\text{ini}} < \eta < \eta_1 < 0) \quad (\text{Inflation}) \\ a_{\text{RD}}(\eta) = \alpha \eta & (0 < \eta_2 < \eta) \quad (\text{RD}) \end{cases}, \quad (2.1)$$

where η_{ini} and η_1 denote the beginning and end of inflation, and η_2 the beginning of the RD period. The continuity conditions for the scale factor a and its derivative $a' = \partial_\eta a$ at the boundary of the inflation and RD periods give the relations

$$\eta_2 = -\eta_1, \quad \alpha = \frac{1}{H_I \eta_1^2}. \quad (2.2)$$

The Hubble parameter $H = a'/a^2$ is given by

$$H(\eta) = \begin{cases} H_{\text{Inf}}(\eta) = H_I & (\text{Inflation}) \\ H_{\text{RD}}(\eta) = \frac{1}{\alpha \eta^2} = H_I \left(\frac{\eta_2}{\eta}\right)^2 & (\text{RD}) \end{cases}. \quad (2.3)$$

The CMB fluctuations give a constraint $H_I < 3.6 \times 10^{-5} M_{\text{Pl}}$.

We consider a minimally coupled massive scalar field ϕ with a mass m . Quantum fields are expanded as

$$\phi(\eta, x^i) = \int \frac{d^3 k}{(2\pi)^3} \left[a_{\mathbf{k}} u_{\mathbf{k}}(\eta) + a_{-\mathbf{k}}^\dagger u_{-\mathbf{k}}(\eta)^* \right] e^{i\mathbf{k} \cdot \mathbf{x}}, \quad (2.4)$$

where the mode functions $u_{\mathbf{k}}(\eta)$ with the comoving momentum \mathbf{k} are the solutions of the equation of motion, $(\square + m^2)u = 0$, and are chosen to asymptote to positive-frequency modes in the remote past. A vacuum is then defined by $a_{\mathbf{k}}|0\rangle = 0$. The vacuum $|0\rangle$, which is an in-state, evolves as η increases, and

¹In [23], particle content and the degree of classicality were studied in a similar background (de Sitter in inflation, followed by RD, and late-time de Sitter).

if an adiabatic condition is broken, the state gets excited above an adiabatic ground state at each moment η .

In the Robertson-Walker spacetime, the wave equation for $\chi_{\mathbf{k}}(\eta) \equiv a(\eta)u_{\mathbf{k}}(\eta)$ is given by

$$\left[-\partial_\eta^2 + \frac{1}{6}Ra^2 - m^2a^2 \right] \chi_{\mathbf{k}}(\eta) = k^2 \chi_{\mathbf{k}}(\eta) , \quad (2.5)$$

where $k = \sqrt{\mathbf{k}^2}$ and

$$\frac{1}{6}Ra^2 = \frac{a''}{a} = \begin{cases} 2/\eta^2 & (\text{Inflation}) \\ 0 & (\text{RD}) \end{cases} . \quad (2.6)$$

Since the wave equation (2.5) has a form of the Schrödinger equation $[-\partial_\eta^2 + V(\eta)]\chi(\eta) = E\chi(\eta)$, the Klein-Gordon (KG) inner product

$$(\chi_1, \chi_2)_\eta = i(\chi_1^*(\partial_\eta \chi_2) - (\partial_\eta \chi_1^*)\chi_2) \quad (2.7)$$

is preserved. We normalize the wave functions $\chi(\eta)$ in terms of the KG inner product.

2.1 Wave functions in the inflationary period

In the inflationary period, a solution of the wave equation is given by

$$\chi_{\text{BD}}(\eta) = \frac{\sqrt{-\pi\eta}}{2} e^{i(2\nu+1)\pi/4} H_\nu^{(1)}(-k\eta) , \quad (2.8)$$

where $H_\nu^{(1)}$ is the Hankel function of the first kind and

$$\nu = \sqrt{\frac{9}{4} - \left(\frac{m}{H_I}\right)^2} \simeq \frac{3}{2} - \frac{1}{3} \left(\frac{m}{H_I}\right)^2 > 0 \quad (2.9)$$

for $m \ll H_I$. Another solution is given by its complex conjugate. Using an asymptotic form of the Hankel function at $|z| \rightarrow \infty$,

$$H_\nu^{(1)}(z) \rightarrow \sqrt{\frac{2}{\pi z}} e^{i(z - (2\nu+1)\pi/4)} , \quad (2.10)$$

$\chi_{\text{BD}}(\eta)$ is shown to have the Bunch-Davies initial condition

$$\chi_{\text{BD}}(\eta) \rightarrow \frac{e^{-ik\eta}}{\sqrt{2k}} \quad (2.11)$$

at $\eta \rightarrow -\infty$.

For $\eta \rightarrow 0$, on the other hand, the wave function can be approximated by using the expansion formula of the Hankel function $H_\nu^{(1)}(z) = J_\nu(z) + iY_\nu(z)$ near $z = 0$,

$$J_\nu(z) \simeq \frac{1}{\Gamma(\nu+1)} \left(\frac{z}{2}\right)^\nu , \quad Y_\nu(z) \simeq \frac{-1}{\sin(\pi\nu)\Gamma(-\nu+1)} \left(\frac{z}{2}\right)^{-\nu} , \quad (2.12)$$

as

$$\chi_{\text{BD}}(\eta) \simeq \frac{i}{\sqrt{2}} k^{-\frac{3}{2} + \frac{1}{3}} \left(\frac{m}{H_I} \right)^2 (-\eta)^{-1 + \frac{1}{3}} \left(\frac{m}{H_I} \right)^2 . \quad (2.13)$$

This is valid when $k|\eta| = k_{\text{phy}}/H_I < 1$ is satisfied, where the physical momentum in the inflationary period is given by $k_{\text{phy}} = k/a = kH_I|\eta|$. In the massless limit, the wave function $u_{\text{BD}}(\eta) = \chi_{\text{BD}}(\eta)/a_{\text{Inf}}(\eta)$ becomes almost constant in time η , and behaves as $k^{-3/2}$. This is consistent with the $\eta \rightarrow 0$ behavior of the exact massless wave function:

$$\chi_{\text{BD}, m=0} = \frac{1}{\sqrt{2k}} \left(1 - \frac{i}{k\eta} \right) e^{-ik\eta} . \quad (2.14)$$

2.2 Wave functions in the RD period

In the RD period, the wave equation (2.5) is written as

$$\left[\partial_x^2 + \left(q^2 + \frac{x^2}{4} \right) \right] \chi = 0 , \quad (2.15)$$

where we have rescaled the parameters η and k as

$$x \equiv (2\tilde{m})^{1/2} \eta , \quad q \equiv (2\tilde{m})^{-1/2} k , \quad \tilde{m} \equiv \frac{m}{H_I \eta_1^2} . \quad (2.16)$$

Since the Hubble parameter is given by $H = H_I(\eta_1/\eta)^2$, the new parameters x and q have the following physical meaning:

$$x = \sqrt{\frac{2m}{H}} , \quad qx = k\eta = \frac{k_{\text{phy}}}{H} , \quad \frac{q}{x} = \frac{k_{\text{phy}}}{2m} , \quad (2.17)$$

where $k_{\text{phy}} = k/a_{\text{RD}}$ is the physical momentum in the RD period. Equation (2.15) is nothing but the Schrödinger equation in an inverted harmonic oscillator with the Hamiltonian $H = -\partial_x^2 - x^2/4$ and the energy eigenvalue q^2 .

The exact solution can be obtained by analytical continuation of the solution in the harmonic potential, and is given by

$$\chi_{\text{EX}}(x) = ce^{-\pi q^2/4} D_{-1/2-iq^2}(e^{i\pi/4}x) , \quad (2.18)$$

where $c = (2\tilde{m})^{-1/4}$. $D_n(z)$ is the parabolic cylinder function satisfying the Weber differential equation

$$[\partial_z^2 + (n + 1/2 - z^2/4)] D_n(z) = 0 . \quad (2.19)$$

It has the following asymptotic behavior

$$D_n(z) \rightarrow e^{-z^2/4} z^n \quad \text{for } |z| \rightarrow \infty . \quad (2.20)$$

The exact solution (2.18) approaches the WKB-approximated one (2.24) for $x \rightarrow \infty$, as will be seen below.

If the adiabaticity condition is satisfied, the exact wave function is approximated by the WKB wave function:

$$\chi_{\text{WKB}}(x) = c \frac{e^{-i \int \omega dx}}{\sqrt{2\omega}}, \quad \omega = \sqrt{\frac{x^2}{4} + q^2}. \quad (2.21)$$

The integral of $\omega(x)$ is given by

$$\int^x \omega(x) dx = \frac{x}{4} \sqrt{x^2 + 4q^2} + q^2 \ln(x + \sqrt{x^2 + 4q^2}) - q^2 \left(\ln 2 + \frac{1}{2} \right) + \frac{\pi}{8}, \quad (2.22)$$

where the x -independent terms are fixed by comparing them with the asymptotic behavior of the exact wave function. By taking $c = (2\tilde{m})^{-1/4}$, the WKB wave function (2.21) is normalized by the KG inner product with respect to the η -derivative as $(\chi_{\text{WKB}}, \chi_{\text{WKB}})_\eta = 1$.

The adiabaticity condition is given by

$$\epsilon \equiv \left| \frac{\omega'(x)}{\omega^2} \right| = \frac{x}{4(q^2 + x^2/4)^{3/2}} < 1. \quad (2.23)$$

In Figure 1, the curve $\epsilon = 1$ is drawn on the (x, q) plane by a thick solid line. Outside the semicircle, the WKB approximation is valid. Also shown in the figure are the vertical line $m = H$ at $x = \sqrt{2}$, the curve $k_{\text{phy}} = H$ (dashed line), and the tilted line $k_{\text{phy}} = m$ (dot-dashed line).

For $q < x/2$, namely, $k_{\text{phy}} < m$, the WKB wave function (2.21) is further approximated as

$$\chi_{\text{WKB}} \simeq c \frac{e^{-ix^2/4 - iq^2 \ln x - i\pi/8}}{\sqrt{x}}. \quad (2.24)$$

Then the exact wave function (2.18) can be shown to asymptote to the WKB wave function by using (2.20). Note also that $x^2/4 = m/(2H) = mt$ where t is the physical time in the RD period, and the wave function oscillates as e^{-imt} .

For $q > x/2$ (i.e., $k_{\text{phy}} > m$), the WKB wave function is reduced to the plane wave

$$\chi_{\text{WKB}} \simeq ce^{-i(q^2 \ln q - q^2/2 + \pi/8)} \frac{e^{-iqx}}{\sqrt{2q}}. \quad (2.25)$$

Since $qx = k_{\text{phy}}/H = 2k_{\text{phy}}t$, the oscillation behavior $e^{-2ik_{\text{phy}}t}$ is controlled by the momentum, not by the mass.

For small x , we can approximate the exact wave function χ_{EX} of (2.18) by a power series of x . The parabolic cylinder function is expanded as

$$D_{-1/2 - iq^2}(e^{i\pi/4}x) = \sum_{r=0}^{\infty} c_r(q^2)x^r, \quad (2.26)$$

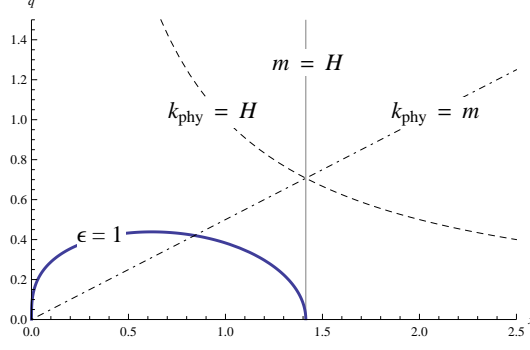


Figure 1: The wave function in the RD period changes its behavior depending on the parameters $x = \sqrt{2m/H}$ (time) and $q = k_{\text{phy}}/\sqrt{2mH}$ (momentum). The thick solid curve represents $\epsilon = 1$; outside the curve, the WKB approximation is valid. The vertical line is $x = \sqrt{2}$, which corresponds to $m = H$ due to (2.17); to the left of the line, $m < H$. The dashed curve is $qx = k_{\text{phy}}/H = 1$; under the curve, $k_{\text{phy}} < H$. The dot-dashed line is $q = x/2$, which corresponds to $k_{\text{phy}} = m$; under the line, $k_{\text{phy}} < m$.

where the first two coefficient functions are given by

$$c_0(q^2) = \frac{2^{-1/4-iq^2/2}\sqrt{\pi}}{\Gamma(3/4+iq^2/2)}, \quad c_1(q^2) = -e^{i\pi/4} \frac{2^{1/4-iq^2/2}\sqrt{\pi}}{\Gamma(1/4+iq^2/2)}. \quad (2.27)$$

The rest of the coefficient functions $c_r(q^2)$ are related to them as, e.g.,

$$\begin{aligned} c_2(q^2) &= -\frac{q^2}{2!}c_0(q^2), \quad c_3(q^2) = -\frac{q^2}{3!}c_1(q^2), \\ c_4(q^2) &= \frac{-1/2+q^4}{4!}c_0(q^2), \quad c_5(q^2) = \frac{-3/2+q^4}{5!}c_1(q^2), \\ c_6(q^2) &= q^2\left(\frac{7/2-q^4}{6!}\right)c_0(q^2), \quad c_7(q^2) = q^2\left(\frac{13/2-q^4}{7!}\right)c_1(q^2). \end{aligned} \quad (2.28)$$

If we take the highest powers of q^2 in each $c_r(q^2)/c_0(q^2)$ and $c_r(q^2)/c_1(q^2)$, the parabolic cylinder function is expanded as

$$\begin{aligned} D_{-1/2-iq^2}(e^{i\pi/4}x) &= c_0(q^2) \left[\cos(qx) + \left(-\frac{1}{2 \cdot 4!}x^4 + \mathcal{O}(x^8)\right) + \left(\frac{7}{2 \cdot 6!}x^4 + \mathcal{O}(x^8)\right)(qx)^2 \right. \\ &\quad \left. + \left(-\frac{11}{8!}x^4 + \mathcal{O}(x^8)\right)(qx)^4 + \left(\frac{25}{10!}x^4 + \mathcal{O}(x^8)\right)(qx)^6 + \dots \right] \\ &+ c_1(q^2)x \left[\frac{\sin(qx)}{qx} + \left(-\frac{3}{2 \cdot 5!}x^4 + \mathcal{O}(x^8)\right) + \left(\frac{13}{2 \cdot 7!}x^4 + \mathcal{O}(x^8)\right)(qx)^2 \right. \\ &\quad \left. + \left(-\frac{17}{9!}x^4 + \mathcal{O}(x^8)\right)(qx)^4 + \left(\frac{35}{11!}x^4 + \mathcal{O}(x^8)\right)(qx)^6 + \dots \right]. \end{aligned} \quad (2.29)$$

For small x , it can be approximated as

$$D_{-1/2-iq^2}(e^{i\pi/4}x) \simeq c_0(q^2) \cos(qx) + c_1(q^2) \frac{\sin(qx)}{q} . \quad (2.30)$$

Since the above expansion turns out to be a double expansion of x^4 and $(qx)^2$, it is a good approximation for small q^2 at $x < 1$. At the same time, since we took the highest orders of q^2 in each $c_r(q^2)$, it should also be a good approximation for large q^2 . Indeed, we have confirmed numerically that the remaining terms in the square brackets in (2.29) decrease and oscillate as a function of qx . This will be related to the fact that the expansion of $(qx)^2$ is an alternative power series. Hence, (2.30) gives a good approximation for small $x \lesssim 1$, irrespective of the magnitude of q .

2.3 Determination of the Bogoliubov coefficients

We now solve the wave equation throughout the inflationary and RD periods by imposing the BD initial condition. The wave function can be written as

$$\chi(\eta) = \begin{cases} \chi_{\text{BD}}(\eta) & \text{(Inflation)} \\ A(k)\chi_{\text{EX}}(\eta) + B(k)\chi_{\text{EX}}^*(\eta) & \text{(RD)} \end{cases} , \quad (2.31)$$

where $\chi_{\text{BD}}(\eta)$ and $\chi_{\text{EX}}(\eta)$ are defined in (2.8) and (2.18).² The Bogoliubov coefficients $A(k)$ and $B(k)$ can be determined by imposing continuity of χ and $\partial_\eta \chi$ at the boundary of the inflationary and RD periods, and are given by

$$\begin{aligned} A(k) &= i [\chi_{\text{EX}}^*(\eta_2) \cdot \partial_\eta \chi_{\text{BD}}(\eta_1) - \partial_\eta \chi_{\text{EX}}^*(\eta_2) \cdot \chi_{\text{BD}}(\eta_1)] , \\ B(k) &= -i [\chi_{\text{EX}}(\eta_2) \cdot \partial_\eta \chi_{\text{BD}}(\eta_1) - \partial_\eta \chi_{\text{EX}}(\eta_2) \cdot \chi_{\text{BD}}(\eta_1)] , \end{aligned} \quad (2.32)$$

where the KG normalization of the wave function $i[\chi_{\text{EX}}^*(\eta_2) \cdot \partial_\eta \chi_{\text{EX}}(\eta_2) - \partial_\eta \chi_{\text{EX}}^*(\eta_2) \cdot \chi_{\text{EX}}(\eta_2)] = 1$ is used. These coefficients satisfy the relation $|A(k)|^2 - |B(k)|^2 = 1$.

The Bogoliubov coefficients $A(k)$ and $B(k)$ in the IR region $k|\eta_1| < 1$ are calculated by using the wave function $\chi_{\text{BD}}(\eta)$ in (2.13). Its derivative is written as

$$\partial_\eta \chi_{\text{BD}}(\eta) \simeq \frac{1 - \frac{1}{3} \left(\frac{m}{H_I} \right)^2}{-\eta} \chi_{\text{BD}}(\eta) \simeq \frac{\chi_{\text{BD}}(\eta)}{-\eta} , \quad (2.33)$$

where $(m/H_I) \ll 1$ was used in the second equality, and (2.32) become

$$\begin{aligned} A(k) &\simeq \left(\frac{\chi_{\text{EX}}^*(\eta_2)}{-\eta_1} - \partial_\eta \chi_{\text{EX}}^*(\eta_2) \right) (i\chi_{\text{BD}}(\eta_1)) , \\ B(k) &\simeq -A(k)^* . \end{aligned} \quad (2.34)$$

² It is an abuse of notation, but we write the wave function in the RD period as $\chi_{\text{EX}}(\eta)$ instead of $\chi_{\text{EX}}(\sqrt{2\tilde{m}}\eta)$ for notational simplicity.

Note that $i\chi_{\text{BD}}(\eta_1)$ is real within this approximation.

Since, at $\eta = \eta_2$, $x = \sqrt{2\tilde{m}}\eta_2 = \sqrt{2m/H_I} \ll 1$ is satisfied, we can use the approximation (2.30) for $\chi_{\text{EX}}(\eta_2)$. Then the coefficient $A(k)$ in (2.34) becomes

$$\begin{aligned} A(k) &\simeq \frac{ie^{-\frac{\pi k^2}{8\tilde{m}}}\chi_{\text{BD}}(\eta_1)}{(2\tilde{m})^{1/4}} \frac{c_0^*}{|\eta_1|} \left[(\cos(k\eta_2) + k\eta_2 \sin(k\eta_2)) + \sqrt{2\tilde{m}} \frac{c_1^*}{c_0^*} \left(\frac{\sin(k\eta_2)}{k} - \eta_2 \cos(k\eta_2) \right) \right] \\ &\simeq \frac{ie^{-\frac{\pi k^2}{8\tilde{m}}}\chi_{\text{BD}}(\eta_1)}{(2\tilde{m})^{1/4}} \frac{c_0^*}{|\eta_1|}, \end{aligned} \quad (2.35)$$

where $k\eta_2 < 1$ and $\sqrt{2\tilde{m}}\eta_2 \ll 1$ were used in the second equality.

2.4 Behaviors of the wave functions with BD initial condition

By using the Bogoliubov coefficients $A(k)$ and $B(k)$, the wave function $u(\eta)$ in the RD period with the BD initial condition is given by

$$\begin{aligned} u(\eta) &= -\frac{iH_I}{\sqrt{2}} k^{-\frac{3}{2}+\frac{1}{3}} \left(\frac{m}{H_I}\right)^2 (-\eta_1)^{\frac{1}{3}} \left(\frac{m}{H_I}\right)^2 \\ &\times \frac{e^{-\pi k^2/4\tilde{m}}}{\sqrt{2\tilde{m}}\eta} 2\Im \left[c_0^* D_{-\frac{1}{2}-i\frac{k^2}{2\tilde{m}}} (e^{i\pi/4}\sqrt{2\tilde{m}}\eta) \right], \end{aligned} \quad (2.36)$$

where c_0 is defined in (2.27). This is one of the main results of the paper, and gives a starting point to calculate the EMT in the RD period. This expression is valid for IR modes with momentum $k|\eta_1| = k\eta_2 < 1$. For UV modes with $k|\eta_1| > 1$, the wave function is not enhanced like this.

For early times $x = \sqrt{2\tilde{m}}\eta = \sqrt{2m/H} \lesssim 1$, the exact solution $\chi_{\text{EX}}(\eta)$ is approximated by (2.30), and the wave function $u(\eta)$ is simplified as

$$u(\eta) \simeq \frac{iH_I}{\sqrt{2}} k^{-\frac{3}{2}+\frac{1}{3}} \left(\frac{m}{H_I}\right)^2 (-\eta_1)^{\frac{1}{3}} \left(\frac{m}{H_I}\right)^2 \frac{\sin(k\eta)}{k\eta}. \quad (2.37)$$

Here we have used the identity

$$2e^{-\pi k^2/4\tilde{m}} \Im(c_0^* c_1) = -1, \quad (2.38)$$

which can be proved by using the property of the KG inner product $(\chi_{\text{EX}}, \chi_{\text{EX}})_\eta = 1$ at $\eta = 0$. For $k\eta < 1$, $u(\eta)$ becomes almost constant, i.e., *frozen*.

For later times $x \gtrsim \sqrt{2}$, the WKB approximation becomes valid, and the wave function $u(\eta)$ is written as

$$\begin{aligned} u(x) &\simeq -\frac{iH_I(2\tilde{m})^{-\frac{3}{4}+\frac{1}{6}} \left(\frac{m}{H_I}\right)^2}{\sqrt{2}} q^{-\frac{3}{2}+\frac{1}{3}} \left(\frac{m}{H_I}\right)^2 (-\eta_1)^{\frac{1}{3}} \left(\frac{m}{H_I}\right)^2 \\ &\times \frac{e^{-\pi q^2/4}}{x} 2\Im \left[c_0^* \frac{e^{-i\int^x \omega dx}}{\sqrt{2\omega}} \right]. \end{aligned} \quad (2.39)$$

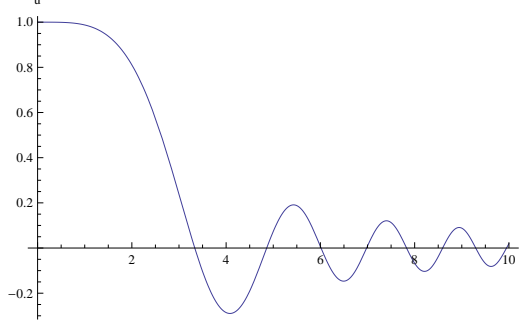


Figure 2: The behavior of the wave function $u(x)$ in (2.36), normalized by $(iH_I/\sqrt{2})k^{-\frac{3}{2}+\frac{1}{3}}\left(\frac{m}{H_I}\right)^2(-\eta_1)^{\frac{1}{3}}\left(\frac{m}{H_I}\right)^2$. The momentum is set to $k = 0$. The wave function is frozen until $x \sim \sqrt{2}$ (i.e., $m \sim H$) and then starts to oscillate.

The WKB approximation is also valid for the UV modes (outside of the semi-circle in Figure 1) even at early times $x < \sqrt{2}$.

As we saw previously, the WKB wave function has two different behaviors, (2.25) at $q > x/2$ ($k_{\text{phy}} > m$), and (2.24) at $q < x/2$ ($k_{\text{phy}} < m$). In the region $q > x/2$, it can be shown numerically that the x -independent phase in the square brackets in (2.39) vanishes for large $q > 1$ and (2.39) becomes identical with (2.37). In contrast, for $q < x/2$, the WKB wave function (2.24) oscillates as $\chi_{\text{WKB}} \sim e^{-ix^2/4} = e^{-imt}$.

In Figure 2, the behavior of the wave function of the exact solution in (2.36) is plotted for $q = 0$. As expected, it is almost constant (frozen) for $x \lesssim \sqrt{2}$, and slowly decreases with an oscillation for $x \gtrsim \sqrt{2}$.

3 Evolution of the energy-momentum tensor

In this section, we calculate the EMT (energy-momentum tensor) in the RD period. The physical results that are relevant to the application to the dark energy are summarized in section 4.

The vacuum expectation value of the EMT is given by

$$\rho(\eta) = \frac{1}{a^2} \int \frac{d^3k}{(2\pi)^3} \frac{1}{2} \left[|u'_k(\eta)|^2 + k^2 |u_k(\eta)|^2 + (ma)^2 |u_k(\eta)|^2 \right], \quad (3.1)$$

$$p(\eta) = \frac{1}{a^2} \int \frac{d^3k}{(2\pi)^3} \frac{1}{2} \left[|u'_k(\eta)|^2 - \frac{1}{3} k^2 |u_k(\eta)|^2 - (ma)^2 |u_k(\eta)|^2 \right]. \quad (3.2)$$

The first term in ρ and p is the time-derivative term, which gives the equation of state $w = p/\rho = 1$. The second term is the spacial-derivative term, and

gives $w = -1/3$. The third term is a contribution of the mass term, and gives $w = -1$.

The integrals (3.1) and (3.2) are divergent in the UV region, and need subtraction of the UV divergences. After the subtraction is performed, we simply cut off the integral at the momentum $k = 1/|\eta_1|$, since only those IR modes are enhanced during the inflationary period. (For more details, see Section 6 of Ref. [8].) The conformal anomaly is given by the subtraction term, but its contribution to the EMT is of the order of H^4 and is negligibly small compared to the vacuum fluctuations generated during the inflation of the order of $H_I^2 H^2$, so we will not consider it in the present paper.

3.1 Massless case

Before investigating the massive scalar field, let us first summarize the evolution of the EMT in the massless case studied in Refs. [7, 8]. The wave function with the BD initial condition is given by

$$u(\eta) \simeq \frac{iH_I}{\sqrt{2}} k^{-3/2} \frac{\sin(k\eta)}{k\eta}, \quad (3.3)$$

for $k|\eta_1| < 1$. Then the energy and pressure densities become

$$\begin{aligned} \rho(\eta) &\simeq \frac{H_I^2}{8\pi^2 a^2} \int_{1/|\eta_{\text{ini}}|}^{1/|\eta_1|} k dk [(\partial_y f(y))^2 + f(y)^2]_{y=k\eta}, \\ p(\eta) &\simeq \frac{H_I^2}{8\pi^2 a^2} \int_{1/|\eta_{\text{ini}}|}^{1/|\eta_1|} k dk \left[(\partial_y f(y))^2 - \frac{f(y)^2}{3} \right]_{y=k\eta}, \end{aligned} \quad (3.4)$$

with $f(y) = \sin(y)/y$. The k -integral is performed for momenta with which the wave function is enhanced during the inflation. Hence, if the inflation continues during $\eta \in [\eta_{\text{ini}}, \eta_1]$, the integral region of the comoving momentum is restricted in $k \in [1/|\eta_{\text{ini}}|, 1/|\eta_1|]$. There is no IR divergence in (3.4), and the IR cutoff does not play an important role.

In the RD period, some of the enhanced modes enter the horizon again. The modes with $k < 1/\eta$ are still out of the horizon and are frozen. Then the time-derivative term, the first term in (3.4), vanishes and the spacial-derivative term, the second term in (3.4), gives

$$\rho^{\text{IR}}(\eta) \simeq \frac{H_I^2}{8\pi^2 a^2} \int^{1/\eta} k dk = \frac{H_I^2}{16\pi^2 a^2 \eta^2} = \frac{H_I^2 H^2}{16\pi^2}. \quad (3.5)$$

On the other hand, the UV modes with $k > 1/\eta$ have already entered the horizon and the wave functions are time dependent. In performing the k -integration over $[1/\eta, 1/\eta_2]$, we estimate the oscillating integrals as

$$\int \frac{dy}{y} \sin^2(y), \quad \int \frac{dy}{y} \cos^2(y) \approx \int \frac{dy}{2y}. \quad (3.6)$$

Then the energy and pressure densities contributed from the UV modes become

$$\begin{aligned}\rho^{\text{UV}}(\eta) &\simeq \frac{H_I^2}{8\pi^2 a^2} \int_{1/\eta}^{1/\eta_2} \frac{k dk}{(k\eta)^2} = \frac{H_I^2 H^2}{8\pi^2} \ln\left(\frac{\eta}{\eta_2}\right) = \frac{H_I^2 H^2}{8\pi^2} N_{\text{RD}} , \\ p^{\text{UV}}(\eta) &\simeq \frac{H_I^2}{8\pi^2 a^2} \int_{1/\eta}^{1/\eta_2} \frac{k dk}{(k\eta)^2} \left(\cos^2(k\eta) - \frac{\sin^2(k\eta)}{3} \right) \simeq \frac{\rho^{\text{UV}}}{3} .\end{aligned}\quad (3.7)$$

Here we have dropped higher-order terms with respect to $(k\eta)^{-1}$. We have also defined an e-folding during the RD period,

$$N_{\text{RD}} = \ln \frac{\eta}{\eta_2} = \ln \frac{a(\eta)}{a_{\text{BB}}} , \quad (3.8)$$

where BB stands for the big bang; namely, a_{BB} means the scale factor at the beginning of the RD period or the end of inflation. N_{RD} represents the number of degrees of freedom that were enhanced during the inflation and have already entered the horizon.

The total energy density is given by $\rho = \rho^{\text{IR}} + \rho^{\text{UV}}$, but the UV contribution (3.7) dominates the IR part (3.5) when $N_{\text{RD}} \gtrsim 1$. Thus the equation of state of the vacuum fluctuations generated during the inflation approaches $w = 1/3$ soon after the RD period begins.

3.2 Massive case at early times

We now study the evolution of the EMT in the massive case. In terms of the variables x and q , (3.1) and (3.2) become

$$\rho(\eta) = \frac{\sqrt{2}\tilde{m}^{5/2}}{\pi^2 a^2} \int_{1/x_{\text{ini}}}^{1/x_1} q^2 dq \left[|\partial_x u|^2 + \left(q^2 + \frac{x^2}{4}\right) |u|^2 \right] , \quad (3.9)$$

$$p(\eta) = \frac{\sqrt{2}\tilde{m}^{5/2}}{\pi^2 a^2} \int_{1/x_{\text{ini}}}^{1/x_1} q^2 dq \left[|\partial_x u|^2 - \left(\frac{q^2}{3} + \frac{x^2}{4}\right) |u|^2 \right] , \quad (3.10)$$

where $x_{\text{ini}} = \sqrt{2\tilde{m}}|\eta_{\text{ini}}|$ and $x_1 = \sqrt{2\tilde{m}}|\eta_1| = \sqrt{2m/H_I}$ correspond to the beginning and end of the inflation period. The integration region represents the momentum region where the wave function is amplified.

We first consider the behavior of the EMT at early times $x = \sqrt{2m/H} < 1$. The wave function is approximated by (2.37), and the EMT becomes

$$\begin{aligned}\rho &\simeq \frac{H_I^2 \tilde{m} x_1^{\frac{2}{3}(\frac{m}{H_I})^2}}{4\pi^2 a^2} \int_{1/x_{\text{ini}}}^{1/x_1} dq q^{1+\frac{2}{3}(\frac{m}{H_I})^2} \left[(\partial_y f(y))^2 + \left(1 + \frac{x^2}{4q^2}\right) f(y)^2 \right]_{y=qx} , \\ p &\simeq \frac{H_I^2 \tilde{m} x_1^{\frac{2}{3}(\frac{m}{H_I})^2}}{4\pi^2 a^2} \int_{1/x_{\text{ini}}}^{1/x_1} dq q^{1+\frac{2}{3}(\frac{m}{H_I})^2} \left[(\partial_y f(y))^2 - \left(\frac{1}{3} + \frac{x^2}{4q^2}\right) f(y)^2 \right]_{y=qx} ,\end{aligned}\quad (3.11)$$

where $f(y) = \sin(y)/y$. The kinetic terms, $(\partial_y f(y))^2 + f(y)^2$ in the square brackets, are the same as those of the massless case (3.4), except for an additional power of the momentum q depending on m . But since the kinetic terms are IR convergent, it does not affect the integrals much. Hence, the contribution from the kinetic terms to (3.11) is given by the same form as in the massless case (3.7).

The contribution from the mass term, namely, the term proportional to $(x^2/4q^2)f(y)^2$, would be IR divergent if we used the massless wave function. However, the additional power of the momentum, $q^{\frac{2}{3}(\frac{m}{H_I})^2}$, which comes from the mass deformation of the wave function, reduces the IR divergence. In terms of k and η , the mass-term contribution is written as

$$\rho^{\text{mass}} = \frac{m^2 H_I^2}{8\pi^2} |\eta_1|^{\frac{2}{3}(\frac{m}{H_I})^2} \int_{1/|\eta_{\text{ini}}|}^{1/|\eta_1|} dk k^{-1+\frac{2}{3}(\frac{m}{H_I})^2} f(k\eta)^2. \quad (3.12)$$

Since the function $f(k\eta)$ starts decreasing at $k \sim 1/\eta$, it gives an effective UV cutoff, and we have

$$\rho^{\text{mass}} \simeq \frac{3H_I^4}{16\pi^2} \left(\frac{|\eta_1|}{\eta}\right)^{\frac{2}{3}(\frac{m}{H_I})^2} \left[1 - \left(\frac{\eta}{|\eta_{\text{ini}}|}\right)^{\frac{2}{3}(\frac{m}{H_I})^2}\right] \simeq \frac{3H_I^4}{16\pi^2} \left[1 - e^{-\frac{2}{3}(\frac{m}{H_I})^2 N_{\text{eff}}}\right]. \quad (3.13)$$

Here, we have used $m \ll H_I$ and defined an effective e-folding

$$N_{\text{eff}} = \ln \left(\frac{|\eta_{\text{ini}}|}{\eta} \right) = N_{\text{Inf}} - N_{\text{RD}}, \quad (3.14)$$

where

$$N_{\text{Inf}} = \ln \frac{|\eta_{\text{ini}}|}{|\eta_1|} = \ln \frac{a_{\text{BB}}}{a_{\text{ini}}} \quad (3.15)$$

is an e-folding number during the inflation period and N_{RD} is that of the RD period defined in (3.8). Thus N_{eff} represents the number of modes that were enhanced during the inflation period, and are still outside the horizon and frozen at time η .

For sufficiently large N_{eff} , (3.13) becomes $3(H_I/2\pi)^4$. This is nothing but the thermal equilibrium energy at the de Sitter temperature $T = H_I/2\pi$, and is independent of m . In contrast, (3.13) can be approximated by

$$\rho^{\text{mass}} \simeq \frac{m^2}{2} \left(\frac{H_I}{2\pi}\right)^2 N_{\text{eff}}, \quad (3.16)$$

when the effective e-folding number satisfies $N_{\text{eff}} < (H_I/m)^2$. For $m \lesssim H_0$ and $H_I \sim 10^{-5} M_{\text{Pl}}$, this upper bound of N_{eff} becomes $(H_I/m)^2 \gtrsim 10^{110}$. Equation (3.16) is also given by a simple physical argument that in the de Sitter

spacetime, an ultra-light field experiences Brownian motion at temperature $T = H_I/2\pi$. The growth of fluctuation since the initial time in de Sitter space was studied in [24, 25, 26, 27].³ The pressure density is $p^{\text{mass}} = -\rho^{\text{mass}}$ and it gives a candidate for the dark energy. As will be shown in section 4, it can explain the present dark energy if N_{eff} satisfies $N_{\text{eff}} \gtrsim 24\pi^2(M_{\text{Pl}}/H_I)^2 \sim 10^{12}$ for $H_I \sim 10^{-5}M_{\text{Pl}}$.

For a more realistic model of the inflation epoch, which is consistent with the CMB observations, we need to consider deviations from the pure de Sitter space. In the slow-roll approximation, or in cases with a nonzero but constant deceleration parameter $q \equiv -1 + \epsilon \equiv -1 - \dot{H}/H^2$, the fluctuations of the field become

$$\langle \phi^2 \rangle \propto \int_{a_{\text{ini}}}^a d(\ln a) H^2 \quad (3.17)$$

(see, e.g., Ref. [29, 34] and H. Kitamoto, private communication), and the result (3.16) is modified accordingly. However, as long as we consider a slight deviation from the de Sitter space that is required by the CMB data, our results do not change considerably.

3.3 Massive case at late times

We then consider the behaviors of the EMT at late times $x = \sqrt{2m/H} > \sqrt{2}$. In this parameter region, the WKB approximation becomes valid, and we can use the wave function (2.39). In performing the momentum integration for the EMT, we divide the integration region into two: the UV region $q > x/2$, which corresponds to $k_{\text{phy}} > m$, and the IR region $q < x/2$, corresponding to $k_{\text{phy}} < m$.

In the UV region with $q > x/2$, the WKB wave function is reduced to the plane wave $\propto e^{-iqx}$ in (2.25). As we discussed below Eq. (2.39), the WKB wave function with the BD initial condition (2.39) becomes identical with (2.37). Then the EMT reduces to (3.11), except for the integration region, where the lower bound of the integration region is replaced by $q = x/2$. Since we are considering the UV region $q > x/2$, the terms proportional to $x^2/4q^2$ in (3.11) can be neglected. Then the UV contribution to (3.11) becomes

$$\begin{aligned} \rho^{\text{UV}} &\simeq \frac{H_I^2 H^2}{8\pi^2} \ln \left(\frac{2}{xx_1} \right) \simeq \frac{H_I^2 H^2}{8\pi^2} N_{\text{RD}} , \\ p^{\text{UV}} &\simeq \frac{\rho^{\text{UV}}}{3} , \end{aligned} \quad (3.18)$$

³See also [28, 29, 30, 31, 32, 33] for recent studies.

where we have used

$$\ln \left(\frac{2}{xx_1} \right) = \ln \left(\frac{H_I}{m} \frac{|\eta_1|}{\eta} \right) \simeq N_{\text{RD}} \quad (3.19)$$

at $m \sim H$, or $x \sim \sqrt{2}$. This is slightly different from N_{RD} defined in (3.8), since the integration is cut off at $q = x/2$ ($k_{\text{phy}} = m$), not at $q = 1/x$ ($k_{\text{phy}} = H$). However, the difference is negligible as long as we consider the region $x \sim \sqrt{2}$, or $m \sim H$.

We next consider the IR region, $q < x/2$ (i.e., $k_{\text{phy}} < m$). In this region, the q -dependence of the WKB wave function (2.39) is given by $u \propto q^{-3/2+1/3(m/H_I)^2}$. The other factors in (2.39) have mild q -dependences, and can be approximated by those at $q = 0$.⁴ Then the energy density (3.9) can be evaluated as

$$\begin{aligned} \rho^{\text{IR}} \simeq & \frac{H_I^2 \tilde{m} x_1^{\frac{2}{3}(\frac{m}{H_I})^2}}{4\pi^2 a^2} \left(\frac{\sqrt{\pi} 2^{-1/4}}{\Gamma(3/4)} \right)^2 \int_{1/x_{\text{ini}}}^{x/2} dq q^{-1+\frac{2}{3}(\frac{m}{H_I})^2} \\ & \times \left[4 \left(\partial_x \left(\frac{\sin(\frac{x^2}{4} + \frac{\pi}{8})}{x\sqrt{x}} \right) \right)^2 + x^2 \left(\frac{\sin(\frac{x^2}{4} + \frac{\pi}{8})}{x\sqrt{x}} \right)^2 \right]. \end{aligned} \quad (3.20)$$

Here, we have dropped the spacial-derivative terms proportional to q^2 in (3.9) since we are considering the IR region $q < x/2$. Note that the q - and x -dependences of the integrand have been separated in (3.20). The q -integration can be performed as

$$\begin{aligned} \int_{1/x_{\text{ini}}}^{x/2} dq q^{-1+\frac{2}{3}(\frac{m}{H_I})^2} &= \frac{3}{2} \left(\frac{H_I}{m} \right)^2 \left(\frac{x}{2} \right)^{\frac{2}{3}(\frac{m}{H_I})^2} \left(1 - \left(\frac{xx_{\text{ini}}}{2} \right)^{-\frac{2}{3}(\frac{m}{H_I})^2} \right) \\ &\simeq \frac{3}{2} \left(\frac{H_I}{m} \right)^2 \left(1 - e^{-\frac{2}{3}(\frac{m}{H_I})^2 N_{\text{eff}}} \right), \end{aligned} \quad (3.21)$$

where we have used

$$\ln \left(\frac{xx_{\text{ini}}}{2} \right) = \ln \left(\frac{m}{H_I} \frac{\eta}{|\eta_1|} \frac{|\eta_{\text{ini}}|}{|\eta_1|} \right) \simeq -N_{\text{RD}} + N_{\text{Inf}} = N_{\text{eff}} \quad (3.22)$$

at $m \sim H$, or $x \sim \sqrt{2}$.

The square brakckets in (3.20) are calculated as

$$[\dots] = \frac{1}{x} \left(1 - 3x^{-2}s + \frac{9}{2}x^{-4}(1-c) \right) \quad (3.23)$$

⁴ In this approximation, the time dependence of ρ^{IR} is represented by the zero-momentum mode. In Appendix A, we give a simple derivation of the time evolution in the zero-momentum approximation. In Figures 3 and 4, we numerically calculate the time evolution of ρ without using such an approximation for the IR modes.

where

$$\begin{aligned} s &= \sin\left(\frac{x^2}{2} + \frac{\pi}{4}\right) = \sin\left(\frac{m}{H} + \frac{\pi}{4}\right) = \sin\left(2mt + \frac{\pi}{4}\right), \\ c &= \cos\left(\frac{x^2}{2} + \frac{\pi}{4}\right) = \cos\left(\frac{m}{H} + \frac{\pi}{4}\right) = \cos\left(2mt + \frac{\pi}{4}\right). \end{aligned} \quad (3.24)$$

When the higher-order corrections to the WKB approximation (2.21) are included, the wave function $\frac{\sin(\frac{x^2}{4} + \frac{\pi}{8})}{x\sqrt{x}}$, which lies in the parentheses in (3.20), is modified as

$$x^{-3/2} (1 + \mathcal{O}(x^{-4})) \sin\left(\frac{x^2}{4} + \frac{\pi}{8} + \mathcal{O}(x^{-2})\right). \quad (3.25)$$

Then the second term with x^{-2} in (3.23) remains unchanged, but the third term with x^{-4} receives modifications. We thus drop it. Therefore, (3.20) becomes

$$\rho^{\text{IR}} \simeq \frac{H_I^2 m^{1/2} H^{3/2}}{8\pi \Gamma(3/4)^2} \left[1 - \frac{3}{2} \frac{H}{m} s\right] N_{\text{eff}}. \quad (3.26)$$

The time dependence is dominantly given by the overall factor $H^{3/2} \sim a^{-3}$ with an additional oscillation given by the square-bracket factor. Note that it is a non-analytic function of m and the behavior cannot be obtained from the massless theory by perturbation with respect to the mass. An interpolating solution between the early-time behavior (3.16) and the late-time behavior (3.26) can be obtained by the zero-momentum wave function given in Appendix A.

Similarly, one can estimate the pressure density. From (3.10), one obtains almost the same equation as in (3.20), but with the second term in the square brackets having a minus sign. Accordingly, (3.23) is replaced by

$$\frac{1}{x} \left(c - 3x^{-2}s + \frac{9}{2}x^{-4}(1-c)\right), \quad (3.27)$$

and we have

$$p^{\text{IR}} \simeq \frac{H_I^2 m^{1/2} H^{3/2}}{8\pi \Gamma(3/4)^2} \left[c - \frac{3}{2} \frac{H}{m} s\right] N_{\text{eff}}. \quad (3.28)$$

The EMTs, (3.26) and (3.28), decrease as $H^{3/2} \propto a^{-3}$, and the equation of state oscillates as

$$w^{\text{IR}} \simeq \left(c - \frac{3}{2} \frac{H}{m} s\right) / \left(1 - \frac{3}{2} \frac{H}{m} s\right) \simeq c - \frac{3}{2} \frac{H}{m} s(1-c). \quad (3.29)$$

The behavior agrees with our knowledge that, once the scalar field ϕ starts oscillating in the quadratic potential $m\phi^2/2$, it behaves as a dust. Let us see

how these behaviors are consistent with the conservation law of the EMT. The energy and pressure densities behave as

$$\begin{aligned}\rho^{\text{IR}} &\propto x^{-3} \left(1 - \frac{3}{x^2} \sin \left(\frac{x^2}{2} + \frac{\pi}{4} \right) + \mathcal{O}(x^{-4}) \right) , \\ p^{\text{IR}} &\propto x^{-3} \left(\cos \left(\frac{x^2}{2} + \frac{\pi}{4} \right) - \frac{3}{x^2} \sin \left(\frac{x^2}{2} + \frac{\pi}{4} \right) + \mathcal{O}(x^{-4}) \right) .\end{aligned}\quad (3.30)$$

It can be easily shown that they satisfy the conservation law of the EMT

$$\partial_x \rho + 3 \frac{\partial_x a}{a} (\rho + p) = 0 \quad (3.31)$$

up to the order x^{-4} , where $\partial_x a/a = 1/x$. Hence, the energy density decreases as a^{-3} as if it were a pressureless dust although the pressure is nonvanishing but oscillating. To see the consistency at the order x^{-6} and higher, we need to include higher-order corrections to the WKB approximation in (2.21).

The ratio of the UV contribution (3.18) to the IR contribution (3.26) is given by

$$\frac{\rho^{\text{UV}}}{\rho^{\text{IR}}} = \frac{\Gamma(3/4)^2}{\pi} \frac{N_{\text{RD}}}{N_{\text{eff}}} \sqrt{\frac{H}{m}} . \quad (3.32)$$

As we saw at the end of the previous section, $N_{\text{RD}} \sim 60$, and a very large e-folding $N_{\text{eff}} \gtrsim 10^{12}$ is necessary. Note also that $m > H$ is satisfied for the late times. Therefore the r.h.s. in (3.32) is much smaller than one, and the IR contribution ρ^{IR} gives a dominant contribution to the EMT compared to ρ^{UV} .

In Figure 3, we numerically performed the q -integrations of (3.9) and (3.10) for the WKB wave function (2.39) with (2.21), and plotted the time evolution of the energy and pressure densities on the left. The equation of state is plotted on the right. The energy and pressure densities are normalized by

$$\frac{H_I^2 \tilde{m}(x_1)^{\frac{2}{3} \left(\frac{m}{H_I} \right)^2}}{4\pi^2 a^2} x^2 = \frac{(x_1)^{\frac{2}{3} \left(\frac{m}{H_I} \right)^2}}{2\pi^2} H_I^2 m^2 \simeq \frac{1}{2\pi^2} H_I^2 m^2 . \quad (3.33)$$

The integration region is taken as $q \in [q_{\text{min}}, x/2]$ to obtain the IR contribution. The lower bound corresponds to

$$q_{\text{min}} = \frac{1}{x_{\text{ini}}} \simeq e^{-N_{\text{eff}}} . \quad (3.34)$$

We set the lower bound of the q -integration to $q_{\text{min}} = 0.001$ for the upper panels and $q_{\text{min}} = 0.8$ for the lower. The behavior of the upper panels agrees well with the analytical estimations given in this section. The energy density decreases with x^{-3} and the equation of state oscillates between -1 and 1 . By taking various values of q_{min} as 10^{-1} , 10^{-2} , 10^{-3} , 10^{-4} , 10^{-5} , etc, we have also confirmed that the magnitude of ρ^{IR} and p^{IR} scales as $N_{\text{eff}} = -\ln(q_{\text{min}})$, as

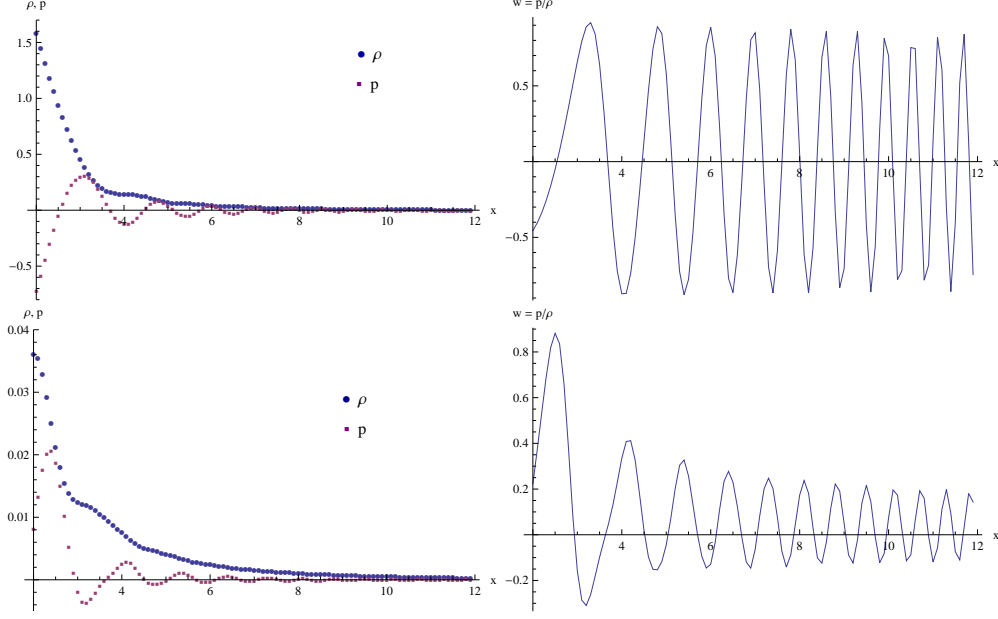


Figure 3: Time evolution of the EMT, given by the IR modes of the WKB wave function, at late times. The horizontal axis represents time $x = (2\tilde{m})^{1/2}\eta = \sqrt{2m/H}$, in the region $x > 2$. The left panels show ρ^{IR} and p^{IR} , normalized by $(H_I m)^2/(2\pi^2)$. The right panels show the equation of state $w^{\text{IR}} = p^{\text{IR}}/\rho^{\text{IR}}$. The integration region over q is taken to be $q \in [q_{\min}, x/2]$, with $q_{\min} = 0.001$ and 0.8 in the upper and lower panels, respectively.

shown by (3.26) and (3.28). On the other hand, if we take the IR cutoff larger, the approximation that the oscillation frequency of the integrand is independent of the momentum in the IR region is invalidated. Then, by summing various modes with different momenta, the oscillating behavior in the time direction is incoherently averaged and is expected to be diminished. Indeed, in the lower panels, the magnitude of p , and, accordingly, w , decreases. However, even in these large q_{\min} , the oscillating behavior of w still remains. In the real setting, as we saw before, we need large $N_{\text{eff}} \sim 10^{12}$, and thus small $q_{\min} \sim e^{-10^{12}}$ is required. Hence, the equation of state w oscillates between $w = -1$ and 1 rather than diminishes.

3.4 Numerical results for the evolution of EMT

In order to see how the early- and late-time behaviors are smoothly connected, we evaluate the evolution of the EMT by using the exact solution (2.36)⁵ in-

⁵*Exact* means that the exact wave function in the RD period is used. For the Bogoliubov coefficient, we used an approximation (2.35).

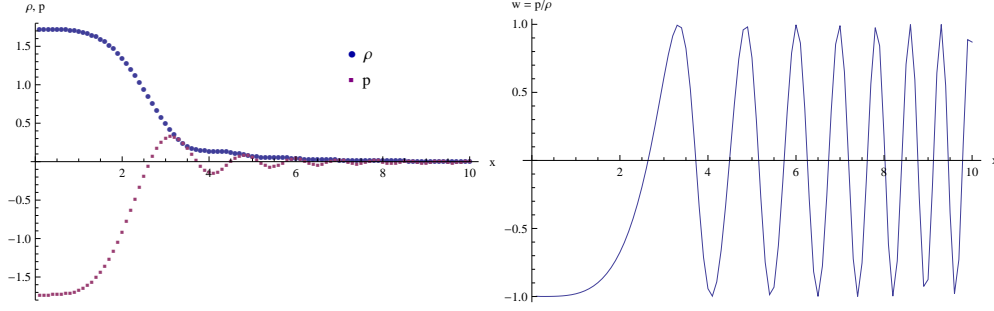


Figure 4: Similar plots to Figure 3, but using the exact wave function in (2.36). Note that the horizontal axis runs from $x = 0$, unlike $x = 2$ in Figure 3. The integration region over q is taken to be $q \in [10^{-5}, 10^{-2}]$. At early times, the IR wave function is frozen and the IR part of the EMT behaves like the dark energy with $w = -1$.

stead of the WKB approximation. We insert the wave function (2.36) into the EMTs, (3.9) and (3.10), and perform numerical integration over q . In order to see the contributions from the IR modes, we set the integration region as $q \in [10^{-5}, 10^{-2}]$. The results are shown in Figure 4, where ρ^{IR} and p^{IR} are normalized by the factor (3.33), as in Figure 3.

For $x > \sqrt{2}$, the results of the exact solution in Figure 4 agree with those of the WKB wave function given in Figure 3. For $x < 1$, w approaches -1 , which agrees with the previous results given in section 3.2. The early-time behavior at $x < 1$ is smoothly connected with the late-time behavior at $x > \sqrt{2}$.

For technical reasons, the numerical integrations are performed in a restricted region of $q > 10^{-5}$ and $q < 10^3$. In order to integrate over $q \in [q_{\text{min}}, q_{\text{max}}]$, where $q_{\text{min}} \sim e^{-N_{\text{eff}}} < e^{-10^{12}}$ and $q_{\text{max}} = x_1^{-1} = (2m/H_I)^{-1/2} \sim 10^{30}$, we use the analytical results based on the approximations of the wave function discussed in the previous sections.

4 Vacuum fluctuations as dark energy

We now investigate possibilities for the vacuum fluctuations of the ultra-light scalar to explain the dark energy at present. We give conditions for the mass and the e-folding number, and then discuss how the EMT evolves through the RD and MD periods. We consider two scenarios. In section 4.1, the ordinary inflation model is discussed. In section 4.2, a double inflation model is considered, where we assume another inflation with a larger Hubble parameter $H_P \sim M_{\text{Pl}}$ before the ordinary inflation starts.

4.1 Ordinary inflation model

We first summarize how the EMT of an ultra-light scalar field evolves in the RD period. In the ordinary inflation model, the enhanced mode during the inflation with the largest momentum soon enters the horizon after the inflation ends. Hence, the EMT is given by a sum of UV and IR contributions. At early times with $m \lesssim H$, as discussed in section 3.2, the EMT is approximately given by $\rho = \rho^{\text{UV}} + \rho^{\text{IR}}$ and $p = p^{\text{UV}} + p^{\text{IR}}$, where

$$\rho^{\text{UV}} = \frac{1}{8\pi^2} H_I^2 H^2 N_{\text{RD}} , \quad p^{\text{UV}} = \frac{1}{3} \rho^{\text{UV}} , \quad (4.1)$$

$$\rho^{\text{IR}} = \frac{1}{8\pi^2} H_I^2 m^2 N_{\text{eff}} , \quad p^{\text{IR}} = -\rho^{\text{IR}} . \quad (4.2)$$

The UV modes have already entered the horizon. N_{RD} represents the number of UV degrees of freedom. Hence, it is time dependent. For the UV modes, the kinetic terms in the EMT mainly contribute and $w = 1/3$ is obtained. The IR modes are still out of the horizon and frozen. Hence, the mass term mainly contributes to the EMT, and we have $w = -1$.

If the mass of the scalar field is heavier than the Hubble parameter at the matter-radiation equality, $m > H_{\text{eq}} = 10^{-28} \text{eV}$, the condition $m \gtrsim H$ becomes satisfied in the late RD period, and the EMT is described by the late-time behaviors discussed in section 3.3. The coherent oscillation (the motion of the zero mode) gradually starts and the behavior (4.2) of the EMT is changed to (3.26) and (3.28):

$$\rho^{\text{IR}} = R \left[1 - \frac{3}{2} \frac{H}{m} s \right] , \quad p^{\text{IR}} = R \left[c - \frac{3}{2} \frac{H}{m} s \right] , \quad (4.3)$$

where s and c are defined in (3.24) and

$$R = \frac{H_I^2 m^{1/2} H^{3/2}}{8\pi \Gamma(3/4)^2} N_{\text{eff}} . \quad (4.4)$$

The amplitudes are proportional to $\sqrt{m} H^{3/2}$ and decay as $H^{3/2} \propto a^{-3}$. The EMT behaves like a dust with an oscillating w . The UV contribution (4.1) remains unchanged.

Now let us study the evolution of the EMT in the MD period. If the mass is lighter than H_{eq} , $m < 10^{-28} \text{eV}$, the coherent oscillation of the zero mode of the scalar field has not yet started at the beginning of the MD period. In the early times of the MD period when the condition $m \lesssim H$ is satisfied, the EMT is again written as a sum of the UV and IR contributions, $\rho = \rho^{\text{UV}} + \rho^{\text{IR}}$. The UV part comes from the modes that have already entered the horizon, and is

given by Eq. (7.20) of Ref. [8]:⁶

$$\rho^{\text{UV}} = \frac{1}{8\pi^2} H_I^2 H^2 \left(\frac{a_{\text{eq}}}{a} \right) N_{\text{RD}} , \quad p^{\text{UV}} = \frac{\rho^{\text{UV}}}{3} , \quad (4.5)$$

where a_{eq} and a are the scale factor at the matter-radiation equality and at each time in the MD period, respectively. $N_{\text{RD}} = \ln(a_{\text{eq}}/a_{\text{BB}})$ is the e-folding number during the RD period and is constant in time. Compared to the IR contributions discussed below, this UV contribution ρ^{UV} becomes negligible because of the factor (a_{eq}/a) . The IR part in the EMT has contributions from the kinetic term and the mass term, $\rho^{\text{IR}} = \rho^{\text{IR,kin}} + \rho^{\text{IR,mass}}$. They are evaluated as

$$\rho^{\text{IR,kin}} = \frac{3}{32\pi^2} H_I^2 H^2 , \quad p^{\text{IR,kin}} = 0 , \quad (4.6)$$

$$\rho^{\text{IR,mass}} = \frac{1}{8\pi^2} H_I^2 m^2 N_{\text{eff}} , \quad p^{\text{IR,mass}} = -\rho^{\text{IR,mass}} . \quad (4.7)$$

$\rho^{\text{IR,kin}}$ was obtained in Eq. (7.18) in Ref. [8]. $\rho^{\text{IR,mass}}$ is the same as in (4.2), but N_{eff} takes a slightly different value since it represents the number of degrees of freedom that are still out of the cosmological horizon, and is time dependent. Note that $\rho^{\text{IR,kin}}$ in (4.6) receives larger contributions from the modes with momenta $k \sim \eta^{-1}$ (i.e., $k_{\text{phy}} \sim H$). In contrast, $\rho^{\text{IR,mass}}$ in (4.7) has dominant contributions from the modes with much lower momenta. It is amusing that a single ultra-light scalar simultaneously contains the dark-energy-like component $\rho^{\text{IR,mass}}$ and the dark-matter-like component $\rho^{\text{IR,kin}}$.

At later times in the MD period, when the condition $m \gtrsim H$ is satisfied, the coherent oscillation starts and the IR contribution is changed. As shown in Appendix A, if time evolution is represented by the zero-momentum approximation, the energy and pressure densities are given by (A.9) and (A.10):

$$\rho^{\text{IR}} \simeq R' \left[1 - \frac{3}{2} \frac{H}{m} s \right] , \quad p^{\text{IR}} \simeq R' \left[c - \frac{3}{2} \frac{H}{m} s \right] \quad (4.8)$$

where s and c are defined in (A.11) and

$$R' = \frac{9}{32\pi^2} H_I^2 H^2 N_{\text{eff}} . \quad (4.9)$$

The amplitude of the energy density decreases as $H^2 \propto a^{-3}$. The interpolating solution between the early-time behavior (4.7) and the late-time behavior (4.8) is obtained in (A.9) and (A.10) in Appendix A.

⁶In [8], a massless case was studied, but, at early times with $m < H$, the wave function is not modified much by the mass.

A dark-energy candidate is given by (4.7). We need three conditions for (4.7) to explain the dark energy in the present universe:

$$\begin{cases} \text{(C1): } m < H_0 \sim 10^{-33} \text{eV} \\ \text{(C2): } \rho_0^{\text{IR, mass}} > \rho_0^{\text{IR, kin}} \\ \text{(C3): } \rho_0^{\text{IR, mass}} \sim 3M_{\text{Pl}}^2 H_0^2 \end{cases}, \quad (4.10)$$

where 0 denotes the present time. The first condition states that the present time corresponds to the early times before the coherent oscillation of the bosonic field starts. The second condition requires that the mass-term contribution with $w = -1$ dominates over the kinetic-term contribution with $w = 0$. This condition gives a lower bound for the mass (or a lower bound for the effective e-folding). Combining these two conditions, we have

$$\text{(C1, C2): } H_0^2 N_{\text{eff}} > m^2 N_{\text{eff}} > \frac{3}{4} H_0^2. \quad (4.11)$$

The third condition is necessary if the observed magnitude of the present dark energy is given by (4.7). It can be written as

$$\text{(C3): } m^2 N_{\text{eff}} = 24\pi^2 \left(\frac{M_{\text{Pl}}}{H_I} \right)^2 H_0^2. \quad (4.12)$$

Inserting (C3) into (C1, C2), we have the following conditions for H_I and N_{eff} :

$$N_{\text{eff}} > 24\pi^2 \left(\frac{M_{\text{Pl}}}{H_I} \right)^2 > \frac{3}{4}. \quad (4.13)$$

In the ordinary inflation, we already have a constraint from the CMB observation that $H_I < 3.6 \times 10^{-5} M_{\text{Pl}}$. Then the second condition in (4.13) is already satisfied. The first one requires quite a large e-folding:

$$N_{\text{eff}} > 1.8 \times 10^{11}. \quad (4.14)$$

Similar analyses were given in [17], where the lower bound for an e-folding number was given as $N > 10^9$. Taking numerical factors into account, we obtain a slightly different value (4.14). The result (4.14) may indicate that the observed universe with the Hubble radius $1/H_0$ is embedded in a huge universe whose size is $e^{1.8 \times 10^{11}}$ times larger.

In Figure 5, we show the time evolution of the EMT in the RD and MD periods. The upper panels plot the energy density ρ , divided by the critical value ρ_{cr} , while the lower panels plot the equation of state $w = p/\rho$. We use m/H for the horizontal axis to denote time evolution. We used the following numerical values: the Planck scale $M_{\text{Pl}} = 2.4 \times 10^{30} \text{meV}$, the present Hubble

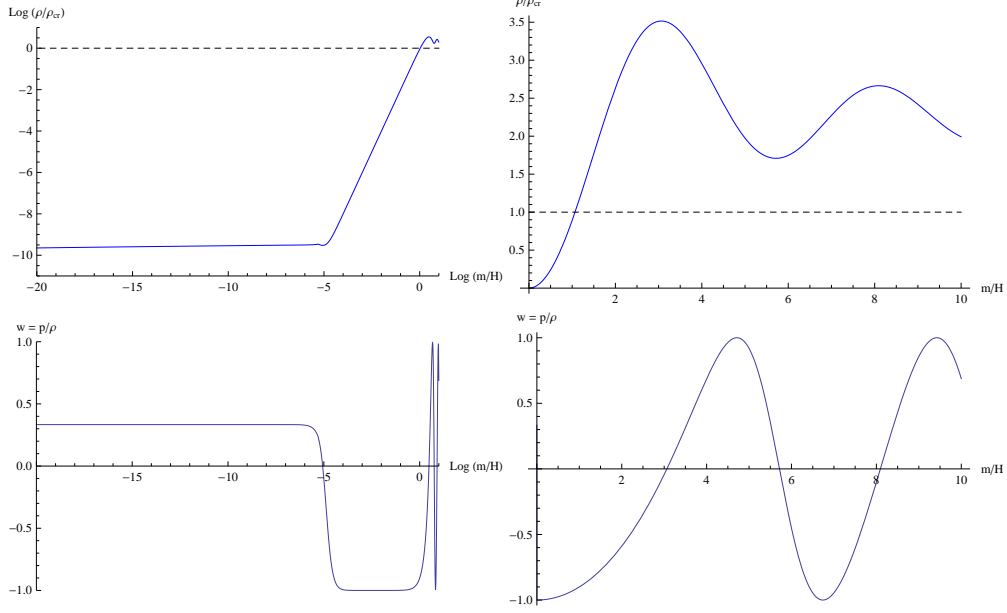


Figure 5: Time evolution of the vacuum fluctuation generated by the ordinary inflation. In the upper panels, the energy density ρ divided by the critical value ρ_{cr} is plotted against time m/H . The dashed line corresponds to the critical value. Both horizontal and vertical axes are logarithmically scaled in the left panel. In the lower panels, the equation of state $w = p/\rho$ is plotted against time m/H . The horizontal axis is logarithmically scaled in the left panel. We used the following numerical values: $H_I = 3.6 \times 10^{-5} M_{\text{Pl}}$, $m = H_0$, and $N_{\text{eff}} = 1.8 \times 10^{11}$. The RD period started at $m/H = 1.6 \times 10^{-56}$, while the left panels display only the region $m/H > 10^{-20}$. The matter-radiation equality occurs at $m/H = 5.0 \times 10^{-6}$, and the present time is $m/H = 1$.

parameter $H_0 = 1.4 \times 10^{-30} \text{meV}$, and the redshift factor at the matter-radiation equality $z_{\text{eq}} = 3.4 \times 10^3$. Thus the Hubble parameter at the equality is given by $H_{\text{eq}} = H_0 z_{\text{eq}}^{3/2} = 2.8 \times 10^{-25} \text{meV}$. In drawing the figures, we chose the Hubble parameter during the inflation at $H_I = 3.6 \times 10^{-5} M_{\text{Pl}} = 8.6 \times 10^{25} \text{meV}$, which is the upper bound of H_I from the CMB constraint. The mass of the ultra-light scalar field is chosen at $m = H_0$. Then condition (C3) in (4.12) requires that $N_{\text{eff}} = 1.8 \times 10^{11}$. For the above parameters, the RD period started at $m/H = H_0/H_I = 1.6 \times 10^{-56}$, the matter-radiation equality occurs at $m/H = H_0/H_{\text{eq}} = 5.0 \times 10^{-6}$, and the present time corresponds to $m/H = H_0/H_0 = 1$.

At early times, the UV contribution to the kinetic term ρ^{UV} is dominant and gives the equation of state $w = 1/3$, while its magnitude is much smaller than the critical value. As time passes, the IR contribution to the mass term

$\rho^{\text{IR,mass}}$ grows and dominates over ρ^{UV} at some time, when w changes to -1 . For the parameters we chose, the transition between the above two behaviors occurs, accidentally, at around the same time as the matter-radiation equality.⁷

As time passes further, the energy density approaches the critical value, which gives the present dark energy, and then w begins to oscillate. As the lower panels in Figure 5 show, the oscillating behavior already begins at present $m/H = 1$ and the present equation of state is given by $w \sim -0.9$. If we choose a smaller mass like $m \sim 0.1H_0$, the equation of state $w = -1$ can be realized at present, but we need a 100 times larger N_{eff} . Such difference will be detected in future observations.

It is also interesting to note that the energy density goes over the critical value when $m > H$, as shown in the upper panels in Figure 5. Indeed, the coefficient of (4.9) is 9/4 times larger than that of (4.7). Then condition (C3) in (4.10) necessarily leads to a situation in which the energy density exceeds the critical density of the background universe in the future. So we need to take into account the back reactions to the geometry to extrapolate our analysis to obtain the behaviors of the future universe.

In [35], it was shown that the vacuum energy of a quantum field drives de Sitter expansion in the inflation period, by studying the back reaction in a self-consistent way. It is also an interesting theoretical problem to study the late-time behavior to understand the fate of the universe. In this case, the interplay between the scale factor and the IR behavior of the wave function, with the Bunch-Davies initial condition, determines the dynamics of the universe self-consistently.

4.2 Double inflation model

Let us now consider another possibility that the EMT of the ultra-light scalar field is enhanced due to the fluctuations created before the ordinary inflation period. As a simple example, we consider a cosmic model with two inflationary periods: the ordinary inflation with the Hubble parameter H_I and a *pre-inflation* with a larger H_P before the ordinary inflation. A similar model was studied to obtain a modified CMB spectrum (see, e.g., [36]). It will be reason-

⁷ Comparing (4.1) and (4.2) with (4.12), we find that the time m/H of this transition is proportional to mH_I . Then, if we choose a smaller H_I , the transition occurs earlier. We also note that the period with $w = 0$ might appear between the eras of $w = 1/3$ and $w = -1$, when $\rho^{\text{IR,kin}}$ in (4.6) is dominant. However, (4.6) could dominate (4.7) with (4.12) when $(H/H_0)^2 > 2.4 \times 10^{11}$, which is actually larger than $(H_{\text{eq}}/H_0)^2 = 3.9 \times 10^{10}$. Since (4.6) appears only in the MD period, the intermediate stage with $w = 0$ never arises for any possible values of the parameters.

able that such a period existed before the ordinary inflation, because, in the very early time of the Planck scale, quantum gravity effects possibly generated a large-Hubble de Sitter expansion. Some concrete examples are the Starobinsky type of inflation [10] and the eternal inflation [37, 38, 39, 40], where our universe is surrounded by a region with a larger Hubble parameter.

In addition to the Hubble parameter in the pre-inflation period H_P , the double inflation model has another important parameter, i.e., the conformal time η_* when the pre-inflation period ended and the ordinary inflation started. As studied in Ref. [8], the wave function is enhanced to a larger amplitude of the order of H_P during the pre-inflation period, and the enhanced modes are restricted within the momentum region $k < 1/|\eta_*|$. If $|\eta_*|$ is larger than the current conformal time η_0 , all the enhanced modes are still outside the current horizon, and do not affect the CMB data. In such a case, H_P is not constrained by the CMB observation, and can be taken as large as the Planck scale M_{Pl} .⁸

We now study the time evolution of the EMT. We first consider the RD period. The EMT is given by a sum $\rho = \rho^{\text{UV}} + \rho^{\text{IR}}$. Here ρ^{UV} is the contribution to ρ from the UV modes that are enhanced during the ordinary inflation, but not during the pre-inflation. Hence, it is given by the same equation as (4.1):

$$\rho^{\text{UV}} = \frac{1}{8\pi^2} H_I^2 H^2 N_{\text{RD}} , \quad p^{\text{UV}} = \frac{1}{3} \rho^{\text{UV}} . \quad (4.15)$$

On the other hand, the IR part ρ^{IR} is the contribution from the IR modes that are greatly enhanced during the pre-inflation with H_P . ρ^{IR} is given by the sum of the mass and the kinetic terms $\rho^{\text{IR}} = \rho^{\text{IR,mass}} + \rho^{\text{IR,kin}}$. Before the coherent oscillation starts, i.e., when $m < H$, the mass term in the EMT becomes

$$\rho^{\text{IR,mass}} = \frac{1}{8\pi^2} H_P^2 m^2 N_{\text{Preinf}} , \quad p^{\text{IR,mass}} = -\rho^{\text{IR,mass}} , \quad (4.16)$$

where

$$N_{\text{Preinf}} = \ln \left| \frac{\eta_{\text{ini}}}{\eta_*} \right| \quad (4.17)$$

is an e-folding number during the pre-inflation period. Here, η_{ini} and η_* denote the conformal time at the beginning and end of the pre-inflation period. The kinetic term in the EMT becomes (see Eq. (8.22) in Ref. [8])

$$\begin{aligned} \rho^{\text{IR,kin}} &= \frac{H_P^2}{32\pi^2 \eta_*^2 a^2} = \frac{H_P^2 H_0^2}{128\pi^2} \left(\frac{\eta_0}{\eta_*} \right)^2 \left(\frac{a_0}{a} \right)^2 = \frac{H_P^2 H_0^2}{128\pi^2} \left(\frac{\eta_0}{\eta_*} \right)^2 z_{\text{eq}}^2 \frac{H}{H_{\text{eq}}} , \\ p^{\text{IR,kin}} &= -\frac{1}{3} \rho^{\text{IR,kin}} . \end{aligned} \quad (4.18)$$

⁸ In Ref. [8], we have also studied the intermediate stage between the pre-inflation and inflation periods. Since the relevant modes are outside the horizon at the intermediate stage, our results are not affected much by this stage, such as by the reheating processes after pre-inflation.

As mentioned above, we assume that all the enhanced modes are out of the current horizon. Thus, they are also always out of horizon and frozen in the past. Hence, the time-derivative term in the EMT vanishes, and the spacial-derivative term gives (4.18) with $w = -1/3$.

In the MD period, the UV contribution becomes negligibly small as in (4.5). At early times ($m \lesssim H$), from the IR contributions, the mass term in the EMT becomes

$$\rho^{\text{IR,mass}} = \frac{1}{8\pi^2} H_P^2 m^2 N_{\text{Preinf}} , \quad p^{\text{IR,mass}} = -\rho^{\text{IR,mass}} . \quad (4.19)$$

At $\eta < |\eta_*|$, the kinetic term in the EMT becomes

$$\rho^{\text{IR,kin}} = \frac{H_P^2 H_0^2}{128\pi^2} \left(\frac{\eta_0}{\eta_*} \right)^2 \left(\frac{H}{H_0} \right)^{4/3} , \quad p^{\text{IR,kin}} = -\frac{1}{3} \rho^{\text{IR,kin}} , \quad (4.20)$$

as in (4.18). On the other hand, at $\eta > |\eta_*|$, some of the enhanced modes have entered the current horizon. Then, as in (4.6), we have

$$\rho^{\text{IR,kin}} = \frac{3}{32\pi^2} H_P^2 H^2 , \quad p^{\text{IR,kin}} = 0 . \quad (4.21)$$

At late times ($m \gtrsim H$), the IR contribution becomes (4.8) and (4.9), with H_I and N_{eff} replaced by H_P and N_{Preinf} . The oscillating behavior of w is obtained again.

As in the ordinary inflation case, (4.19) gives a dark-energy candidate. In order to explain the dark energy in the present universe, the three conditions (4.10) are required. The first and second conditions give

$$(C1, C2) : \quad H_0^2 N_{\text{Preinf}} > m^2 N_{\text{Preinf}} > \frac{1}{16} H_0^2 \left(\frac{\eta_0}{\eta_*} \right)^2 , \quad (4.22)$$

while the third one becomes

$$(C3) : \quad m^2 N_{\text{Preinf}} = 24\pi^2 \left(\frac{M_{\text{Pl}}}{H_P} \right)^2 H_0^2 . \quad (4.23)$$

Inserting (C3) into (C1, C2), we have

$$N_{\text{Preinf}} > 24\pi^2 \left(\frac{M_{\text{Pl}}}{H_P} \right)^2 > \frac{1}{16} \left(\frac{\eta_0}{\eta_*} \right)^2 . \quad (4.24)$$

Since the enhanced modes must be outside the horizon in the present universe, $|\eta_*| > \eta_0/(2\pi)$ needs to be satisfied, which gives $(1/16)(\eta_0/\eta_*)^2 < \pi^2/4$. Then, a large Hubble parameter as $H_P \sim M_{\text{Pl}}$ satisfies the second inequality in (4.24). The first one requires that the e-folding number during the pre-inflation must satisfy

$$N_{\text{Preinf}} > 24\pi^2 \sim 2.4 \times 10^2 . \quad (4.25)$$

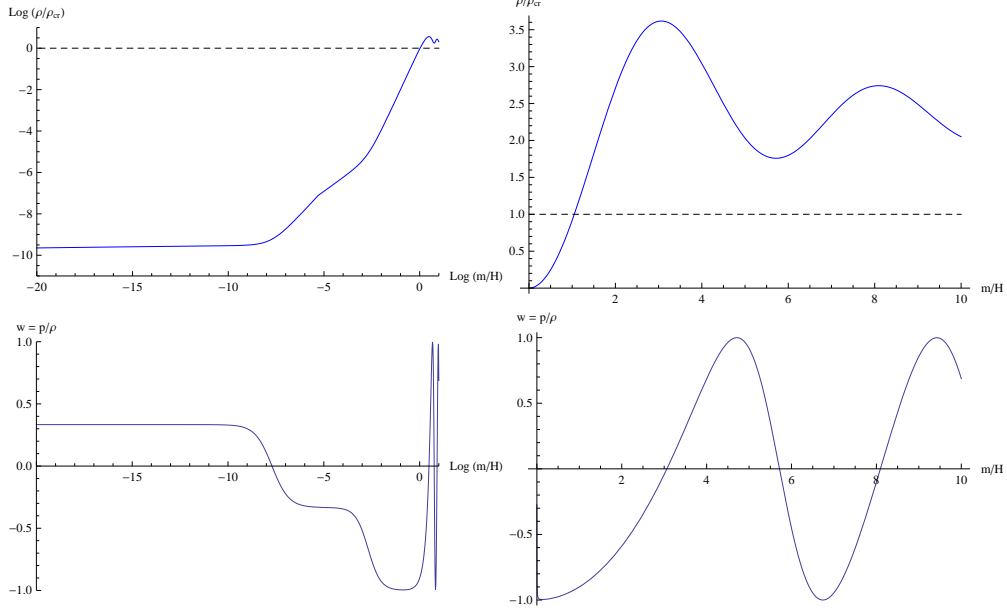


Figure 6: Similar plots to Figure 5, but for the vacuum fluctuations generated by the pre-inflation. The same numerical values are used as in Figure 5. For the additional parameters, we used $H_P = M_{\text{Pl}}$, $|\eta_*| = \eta_0$, and thus $N_{\text{Preinf}} = 2.4 \times 10^2$. Compared to Figure 5, a new state with $w = -1/3$ appears during the transition from $w = 1/3$ to $w = -1$.

Compared to the ordinary inflation, the e-folding number does not need to be as large as (4.14).

In Figure 6, we show the time evolution of the energy density ρ/ρ_{cr} and the equation of state $w = p/\rho$ in the RD and MD periods. We take the same parameters as in Figure 5. For the additional parameters, we use $H_P = M_{\text{Pl}}$ and $|\eta_*| = \eta_0$. Then $N_{\text{Preinf}} = 2.4 \times 10^2$ is required by (4.23).

At early times, the UV contribution to the kinetic term ρ^{UV} is dominant and gives $w = 1/3$, while its magnitude is much smaller than the critical value. As time passes, the IR contribution to the kinetic term $\rho^{\text{IR,kin}}$ dominates, and the era with $w = -1/3$ starts. As time passes further, the IR contribution to the mass term $\rho^{\text{IR,mass}}$ dominates, and the era with $w = -1$ starts. At later times, when $m \gtrsim H$, the era with oscillating w starts.

The existence of the intermediate stage with $w = -1/3$ depends on the values of the free parameters that we take. The transition time m/H from $w = 1/3$ to $w = -1/3$, i.e., when $\rho^{\text{IR,kin}}$ dominates ρ^{UV} , can be shown to be proportional to $m(H_I \eta_*/H_P)^2$, by comparing (4.15) and (4.18). On the other hand, the time m/H when $\rho^{\text{IR,mass}}$ dominates over ρ^{UV} is proportional to

mH_I , by comparing (4.15) and (4.16) with (4.23). Hence, if we choose a larger η_* and/or a smaller H_P , the era with $w = -1$ starts before $w = -1/3$ might start, and thus the intermediate stage with $w = -1/3$ does not arise.

5 Conclusions and discussions

In this paper, we have calculated the time evolution of the energy-momentum tensor of an ultra-light scalar field with a mass $m \lesssim 10^{-33}\text{eV}$. In the case of axion-like particles, the initial condition is set by hand by the misalignment mechanism. We instead assume that the fluctuations generated during de Sitter expansion in the primordial inflation gave the initial condition of the amplitude of the vacuum energy. If the fluctuations are enhanced during the ordinary inflation with the Hubble parameter $H_I \sim 10^{-5}M_{\text{Pl}}$, a very large e-folding $N_{\text{eff}} \sim 10^{12}$ is necessary to explain the dark energy at present. But, if we consider a cosmic history with another Planckian universe with a large Hubble parameter $H_P \sim M_{\text{Pl}}$ before the ordinary inflation, a much smaller e-folding number $N_{\text{eff}} \sim 240$ during the pre-inflation is sufficient. We furthermore calculated how the dark energy evolves in future, though the back reaction to the geometry becomes relevant and needs to be taken in a self-consistent manner. The amplitude decreases as a^{-3} where a is the scale factor, like a dust, and the equation of state oscillates between $w = -1$ and 1 with a large oscillation period $1/m$. If the mass is a bit larger than the current Hubble, e.g., $m = 10^{-32}\text{eV}$, such an oscillatory behavior may be detectable (see, e.g., [41]). In most studies of the quintessence scenario, the classical equation for the zero mode is used to compare with the observational data. It is interesting to extend the analyses to include the nonzero-momentum modes discussed in this paper and to give more detailed observational constraints on the model parameters.

Another important issue not discussed in the present paper is the effect of interactions. In the de Sitter expanding universe, we often encounter IR divergences $\ln(k|\eta|)$ when we calculate loop corrections of various quantities (see, e.g., [42]). The IR divergences are related to the secular time growth of these quantities in the $|\eta| \rightarrow 0$ limit and in many cases they can be resummed. For example, the secular growth in a massless scalar with $\lambda\phi^4$ interactions can be cured by resumming the logarithmic factors so that the massless field acquires an effective mass $m_{\text{eff}}^2 = \lambda/2(H_I/2\pi)^2 N$, where N is an e-folding number [43, 44]. Then such an interaction generates the vacuum energy proportional to $\rho \sim \lambda/8(H_I/2\pi)^4 N^2$. For an infinite N , it approaches an equilibrium value $3H_I^4/16\pi^2$ that is independent of λ . The ratio of this energy density to the critical density of the present universe is given by $\Omega_{\phi^4} \propto \lambda N^2 H_I^4 / (384\pi^4 M_{\text{Pl}}^2 H_0^2)$.

If $H_I = 10^{-5} M_{\text{Pl}}$ and $N = 10^2$, it becomes $\Omega_{\phi^4} \sim \lambda \times 10^{100}$. Hence, unless we take a very small coupling $\lambda \sim 10^{-100}$, it exceeds the critical energy density of the universe. We want to come back to this issue in the future.

Acknowledgements

The authors would like to thank Yasuhiro Sekino for insightful discussions and a collaboration at the early stage of the investigations, and Hiroyuki Kitamoto for useful discussions and comments. This work is supported in part by a Grant-in-Aid for Scientific Research (Nos. 23244057, 23540329, and 24540279) from the Japan Society for the Promotion of Science. This work is also partially supported by “The Center for the Promotion of Integrated Sciences (CPIS)” of Sokendai.

A Time evolution of the zero-momentum mode

In this appendix, we study zero-momentum modes and calculate the EMT by using them. We obtain the time evolution of the EMT in the MD period, which interpolates the early-time (4.7) and late-time behaviors (4.8). We also reproduce the time evolution in the RD period, which interpolates (3.16) and (3.26).⁹

The wave equation, $(\square + m^2)u = 0$, in the Robertson-Walker metric is written as

$$u'' + 2\mathcal{H}u' + (k^2 + (ma)^2)u = 0, \quad (\text{A.1})$$

where $' = \partial_\eta$, $\mathcal{H} = a'/a$, and η is the conformal time. In terms of the physical time t , it is written as

$$\ddot{u} + 3H\dot{u} + ((k/a)^2 + m^2)u = 0, \quad (\text{A.2})$$

with $\dot{} = \partial_t$ and $H = \dot{a}/a$. For sufficiently low-momentum modes, we can neglect the $(k_{\text{phy}})^2 = (k/a)^2$ term in (A.2) and approximate the equation as

$$\ddot{u} + 3H\dot{u} + m^2u = 0. \quad (\text{A.3})$$

We first see the freezing behavior of the low-momentum wave function at early times ($m < H$) in the RD and MD eras. Then, we can neglect the m^2 term in (A.3), which is easily solved as

$$u = F + G \int dt a^{-3}, \quad (\text{A.4})$$

⁹The time evolution of zero-momentum wave function is also investigated in [45] to discuss how an ultra-light scalar affects the growth rate of cosmological perturbation.

where F and G are arbitrary constants. The first term with F is time independent and represents the frozen wave function. Imposing the Bunch-Davies initial condition, $F \neq 0$ and $G = 0$ are chosen. Once these coefficients are fixed by the initial condition, the solution (A.4) continues to be valid throughout the history, either in the RD or MD periods, as long as the condition $k_{\text{phy}}, m \ll H$ is satisfied.

We next consider the case where the scale factor behaves as $a \propto t^p$. Then, the Hubble parameter is given by $H = p/t$ and the solution to Eq. (A.3) is given by using the Bessel functions as

$$u = (mt)^{-\nu} (F' J_\nu(mt) + G' Y_\nu(mt)) , \quad (\text{A.5})$$

where

$$\nu = \frac{3}{2}p - \frac{1}{2} , \quad (\text{A.6})$$

and F' and G' are arbitrary constants. At early times with $mt < 1$, (i.e., $m < H$), we can show, by using the expansion formula (2.12) of the Bessel function near the origin, that the first and second terms in (A.5) give those in (A.4), respectively. In the MD period, $p = 2/3$, $\nu = 1/2$, and (A.5) becomes

$$u = (mt)^{-1} (F'' \sin(mt) + G'' \cos(mt)) , \quad (\text{A.7})$$

where F'' and G'' are arbitrary constants. Note that the solutions (A.5) and (A.7) are good approximations to (A.2) for low-momentum modes with $k_{\text{phy}} \ll m, \sqrt{mH}$, either in early times $mt < 1$ ($m < H$) or in late times $mt > 1$ ($m > H$).

As we studied in section 4, we are interested in the situation where the wave functions continue to be frozen until the MD period and then start oscillating. Then the coefficients F'' and G'' in (A.7) can be determined by requiring that u is constant near $t \sim 0$ and the amplitude is given by the wave function in the RD period (2.37), or, equivalently, by that in the inflation period (2.13). Hence, the wave function in the MD period is given by

$$u = \frac{iH_I}{\sqrt{2}} k^{-\frac{3}{2} + \frac{1}{3}\left(\frac{m}{H_I}\right)^2} (-\eta_1)^{\frac{1}{3}\left(\frac{m}{H_I}\right)^2} \frac{\sin(mt)}{mt} . \quad (\text{A.8})$$

Using this wave function, the EMT becomes

$$\begin{aligned} \rho^{\text{IR}} &= \frac{1}{8\pi^2} H_I^2 \frac{1}{t^2} \left[1 - \frac{1}{mt} s + \frac{1}{2(mt)^2} (1 - c) \right] N_{\text{eff}} \\ &= \frac{9}{32\pi^2} H_I^2 H^2 \left[1 - \frac{3}{2} \frac{H}{m} s + \frac{9}{8} \left(\frac{H}{m} \right)^2 (1 - c) \right] N_{\text{eff}} , \end{aligned} \quad (\text{A.9})$$

$$\begin{aligned}
p^{\text{IR}} &= \frac{1}{8\pi^2} H_I^2 \frac{1}{t^2} \left[c - \frac{1}{mt} s + \frac{1}{2(mt)^2} (1 - c) \right] N_{\text{eff}} \\
&= \frac{9}{32\pi^2} H_I^2 H^2 \left[c - \frac{3}{2} \frac{H}{m} s + \frac{9}{8} \left(\frac{H}{m} \right)^2 (1 - c) \right] N_{\text{eff}} , \quad (\text{A.10})
\end{aligned}$$

where

$$\begin{aligned}
s &= \sin(2mt) = \sin\left(\frac{4m}{3H}\right) , \\
c &= \cos(2mt) = \cos\left(\frac{4m}{3H}\right) . \quad (\text{A.11})
\end{aligned}$$

These expressions are valid either in early times $m < H$ ($mt < 1$) or in late times $m > H$ ($mt > 1$), since the wave function (A.7), and thus (A.8), are valid at both times. Indeed, they give not only the late-time behavior (4.8) but also the early-time behavior (4.7), as can be seen by expanding the trigonometric functions with respect to m/H .

We may consider another scenario where the frozen behavior becomes oscillating in the RD period, as analyzed in section 3. In this case, we can connect the wave function (A.5) in the RD period, with $p = 1/2$ and $\nu = 1/4$, to the wave function in the inflation period (2.13), and obtain

$$u = \frac{iH_I}{\sqrt{2}} k^{-\frac{3}{2} + \frac{1}{3}\left(\frac{m}{H_I}\right)^2} (-\eta_1)^{\frac{1}{3}\left(\frac{m}{H_I}\right)^2} 2^\nu \Gamma(\nu + 1) (mt)^{-\nu} J_\nu(mt) , \quad (\text{A.12})$$

where we have used the expansion formula (2.12) of the Bessel function near the origin. Then, (A.12) reproduces the early-time behavior of the EMT (3.16). The late-time behavior is obtained by using the asymptotic form of the Bessel function

$$J_\nu(z) = \sqrt{\frac{2}{\pi z}} \left[\left(1 + \mathcal{O}(z^{-2})\right) \cos\left(z - \frac{2\nu + 1}{4}\pi\right) + \mathcal{O}(z^{-1}) \sin\left(z - \frac{2\nu + 1}{4}\pi\right) \right] \quad (\text{A.13})$$

at $|z| \gg 1$. It turns out that (A.12) asymptotes to the WKB wave function (2.39) with (2.24), which receives higher-order corrections as in (3.25). Accordingly, we can reproduce the late-time behavior of the EMT, (3.26) and (3.28).

References

- [1] P. A. R. Ade *et al.* [Planck Collaboration], *Astron. Astrophys.* **571**, A16 (2014) [arXiv:1303.5076 [astro-ph.CO]].
- [2] S. Weinberg, *Rev. Mod. Phys.* **61**, 1 (1989).
- [3] T. S. Bunch and P. C. W. Davies, *Proc. Roy. Soc. Lond. A* **360**, 117 (1978).

- [4] J. S. Dowker and R. Critchley, Phys. Rev. D **13**, 3224 (1976).
- [5] P. A. R. Ade *et al.* [Planck Collaboration], Astron. Astrophys. **571**, A22 (2014) [arXiv:1303.5082 [astro-ph.CO]].
- [6] V. Mukhanov, “Physical foundations of cosmology,” Cambridge, UK: Univ. Pr. (2005) 421 p
- [7] D. Glavan, T. Prokopec and V. Prymidis, Phys. Rev. D **89**, 024024 (2014) [arXiv:1308.5954 [gr-qc]].
- [8] H. Aoki, S. Iso and Y. Sekino, Phys. Rev. D **89**, 103536 (2014) [arXiv:1402.6900 [hep-th]].
- [9] D. Glavan, T. Prokopec and D. C. van der Woude, Phys. Rev. D **91**, no. 2, 024014 (2015) [arXiv:1408.4705 [gr-qc]].
- [10] A. A. Starobinsky, Phys. Lett. B **91**, 99 (1980).
- [11] J. A. Frieman, C. T. Hill, A. Stebbins and I. Waga, Phys. Rev. Lett. **75**, 2077 (1995) [astro-ph/9505060].
- [12] A. Arvanitaki, S. Dimopoulos, S. Dubovsky, N. Kaloper and J. March-Russell, Phys. Rev. D **81**, 123530 (2010) [arXiv:0905.4720 [hep-th]].
- [13] R. Hlozek, D. Grin, D. J. E. Marsh and P. G. Ferreira, Phys. Rev. D **91**, no. 10, 103512 (2015) [arXiv:1410.2896 [astro-ph.CO]].
- [14] J. E. Kim, arXiv:1409.3609 [astro-ph.CO].
- [15] J. E. Kim, Y. Semertzidis and S. Tsujikawa, Front. Phys. **2**, 60 (2014) [arXiv:1409.2497 [hep-ph]].
- [16] S. Tsujikawa, Class. Quant. Grav. **30**, 214003 (2013) [arXiv:1304.1961 [gr-qc]].
- [17] C. Ringeval, T. Suyama, T. Takahashi, M. Yamaguchi and S. Yokoyama, Phys. Rev. Lett. **105**, 121301 (2010) [arXiv:1006.0368 [astro-ph.CO]].
- [18] V. F. Mukhanov, L. R. W. Abramo and R. H. Brandenberger, Phys. Rev. Lett. **78**, 1624 (1997) [gr-qc/9609026].
- [19] L. R. W. Abramo, R. H. Brandenberger and V. F. Mukhanov, Phys. Rev. D **56**, 3248 (1997) [gr-qc/9704037].
- [20] L. R. W. Abramo, Phys. Rev. D **60**, 064004 (1999) [astro-ph/9903270].

- [21] E. W. Kolb, S. Matarrese, A. Notari and A. Riotto, Phys. Rev. D **71**, 023524 (2005) [hep-ph/0409038].
- [22] E. Barausse, S. Matarrese and A. Riotto, Phys. Rev. D **71**, 063537 (2005) [astro-ph/0501152].
- [23] S. Singh, S. K. Modak and T. Padmanabhan, Phys. Rev. D **88**, 125020 (2013) [arXiv:1308.4976 [gr-qc]].
- [24] A. D. Linde, Phys. Lett. B **116**, 335 (1982).
- [25] A. A. Starobinsky, Phys. Lett. B **117**, 175 (1982).
- [26] A. Vilenkin and L. H. Ford, Phys. Rev. D **26**, 1231 (1982).
- [27] A. D. Linde, “Particle physics and inflationary cosmology,” Harwood, Chur, Switzerland, 1990, [hep-th/0503203].
- [28] F. Finelli, G. Marozzi, G. P. Vacca and G. Venturi, Phys. Rev. D **65**, 103521 (2002) [gr-qc/0111035].
- [29] F. Finelli, G. Marozzi, A. A. Starobinsky, G. P. Vacca and G. Venturi, Phys. Rev. D **79**, 044007 (2009) [arXiv:0808.1786 [hep-th]].
- [30] F. Finelli, G. Marozzi, A. A. Starobinsky, G. P. Vacca and G. Venturi, Phys. Rev. D **82**, 064020 (2010) [arXiv:1003.1327 [hep-th]].
- [31] G. Marozzi, M. Rinaldi and R. Durrer, Phys. Rev. D **83**, 105017 (2011) [arXiv:1102.2206 [astro-ph.CO]].
- [32] H. Kitamoto and Y. Kitazawa, Phys. Rev. D **83**, 104043 (2011) [arXiv:1012.5930 [hep-th]].
- [33] H. Kitamoto and Y. Kitazawa, Phys. Rev. D **85**, 044062 (2012) [arXiv:1109.4892 [hep-th]].
- [34] T. M. Janssen, S. P. Miao, T. Prokopec and R. P. Woodard, Class. Quant. Grav. **25**, 245013 (2008) [arXiv:0808.2449 [gr-qc]].
- [35] Y. Habara, H. Kawai and M. Ninomiya, JHEP **1502**, 148 (2015) [arXiv:1410.0644 [hep-th]].
- [36] J. Silk and M. S. Turner, Phys. Rev. D **35**, 419 (1987).
- [37] S. R. Coleman and F. De Luccia, Phys. Rev. D **21**, 3305 (1980).
- [38] S. W. Hawking and I. G. Moss, Phys. Lett. B **110**, 35 (1982).

- [39] A. D. Linde, Phys. Lett. B **175**, 395 (1986).
- [40] B. Freivogel, Y. Sekino, L. Susskind and C. -P. Yeh, Phys. Rev. D **74**, 086003 (2006) [hep-th/0606204].
- [41] D. J. E. Marsh, P. Bull, P. G. Ferreira and A. Pontzen, Phys. Rev. D **90**, no. 10, 105023 (2014) [arXiv:1406.2301 [astro-ph.CO]].
- [42] T. Tanaka and Y. Urakawa, Class. Quant. Grav. **30**, 233001 (2013) [arXiv:1306.4461 [hep-th]].
- [43] A. A. Starobinsky and J. Yokoyama, Phys. Rev. D **50**, 6357 (1994) [astro-ph/9407016].
- [44] C. P. Burgess, L. Leblond, R. Holman and S. Shandera, JCAP **1003**, 033 (2010) [arXiv:0912.1608 [hep-th]].
- [45] D. J. E. Marsh and P. G. Ferreira, Phys. Rev. D **82**, 103528 (2010) [arXiv:1009.3501 [hep-ph]].